Complex basal conditions and their influence on ice flow at the onset of the Northeast Greenland Ice Stream

Steven Franke[1], Daniela Jansen[1], Sebastian Beyer[1,2], Tobias Binder*[1], John Paden[3], and Olaf Eisen[1,4]

[1]Alfred Wegener Institute, Helmholtz Centre for Polar and Marine Research, Bremerhaven, Germany
[2]MARUM - Center for Marine Environmental Sciences, University of Bremen, Bremen, Germany
[3]Center for Remote Sensing of Ice Sheets (CReSIS), University of Kansas, Lawrence, KS, USA
[4]Department of Geosciences, University of Bremen, Bremen, Germany

Key Points

- Basal roughness at the onset of the NEGIS hints to a geomorphic anisotropy and a change in the geomorphological regime
- Basal water is funnelled into the ice stream upstream and redistributed towards the shear margins further downstream
- A smooth and progressively lubricated bed reduces basal traction and favours the acceleration of the NEGIS at its onset

*now at Ibeo Automotive Systems, Hamburg, Germany

Abstract

The ice stream geometry and large ice surface velocities at the onset region of the Northeast Greenland Ice Stream (NEGIS) are not yet well reproduced by ice sheet models. They are a significant source of uncertainty in present ice sheet projections towards their future contribution to sea-level rise. The quantification of basal sliding and a parametrisation of basal conditions remains a major gap. In this study, we assess the basal conditions of the onset region of the NEGIS in a systematic analysis of airborne ultra-wideband radar data. We evaluate basal roughness and basal return echoes in the context of the current ice stream geometry and ice surface velocity. We observe a change from a smooth to a rougher bed where the ice stream widens, and a distinct roughness anisotropy, indicating a preferred orientation of subglacial structures. In this region, we also find an apparent increase of the bed return power towards the centre of the ice stream, potentially indicating increased water content at the base. At the downstream part, we observe an increased bed return power throughout the entire width of the ice stream and outside its margins. Together with basal water routing pathways, this hints to two different zones in this part of NEGIS: the upstream region collecting water, reducing basal traction, and in the further downstream part the distribution of basal water underneath and beyond the shear margins. Our findings support the hypothesis that the NEGIS is strongly controlled by the subglacial water system in its onset region.

Plain Language Summary

The Northeast Greenland Ice Stream (NEGIS) transports a large amount of ice mass from the interior of the Greenland Ice Sheet (GrIS) towards the ocean. The extent and geometry of the NEGIS are difficult to reproduce in current ice sheet models because many boundary conditions, such as the properties of the ice base, are not well known. In this study, we present new characteristics of the ice base from the onset region of the NEGIS derived by airborne radio-echo sounding data. Our data yield a smooth and increasingly lubricated bed in the upstream part of our survey area, which enables the ice to accelerate. Our results confirm the hypothesis that the position of the ice stream boundaries are coupled to the subglacial hydrology system. In a warming climate, more meltwater can potentially drain towards higher elevations and could thus favor the initiation of faster ice flow in central Greenland.

Introduction

The lack of high-resolution bed topography and knowledge about the subglacial conditions in Greenland and Antarctica is one of the largest sources of uncertainty in present ice sheet projections (Morlighem et al., 2019) and higher resolution of bed topography is needed to improve the accuracy of ice sheet models (Durand et al., 2011). The subglacial environment of the Antarctic and Greenland Ice Sheet (AIS, GrIS) is only poorly known from direct observations. The technical and logistical efforts for an analysis of the base underneath ice, often several kilometres thick, is much more challenging than observations on paleo-glaciated areas on land or the seafloor through remote sensing techniques (e.g. Stokes et al. (2013); Clark and Meehan (2001)) or marine swath bathymetry (e.g. Arndt et al. (2019); Dowdeswell et al. (2004)). Most of the knowledge about the ice covered bathymetry, bed topography and basal properties are deduced from the analysis and interpretation of indirect observations like radio-echo sounding (Fretwell et al., 2013; Humbert et al., 2018; Morlighem

et al., 2017, 2019; Schroeder et al., 2020, 2019; Winter et al., 2017), seismic (Brisbourne et al., 2014; Dow et al., 2013; Hofstede et al., 2018; Kulessa et al., 2017; Rosier et al., 2018; Smith et al., 2020) as well as magnetic and gravimetric surveys combined with modelling approaches (An et al., 2019; Cochran and Bell, 2012; Muto et al., 2013; Eisermann et al., 2020). In the central regions of the AIS and GrIS, little is known about the distribution and properties of bedrock, lithified and unlithified sediments, liquid water quantity, hydromechanical processes and the thermal and mechanical properties of ice (Clarke, 2005). Variations of these parameters over time can influence the spatial and temporal behaviour of the ice sheets and their streams, by altering the fast flow dynamics or the mobilisation of subglacial sediments. It is assumed that parts of the base of the GrIS are covered by mechanically weak sediments, which facilitate basal sliding (Christianson et al., 2014; Dow et al., 2013). Furthermore, an analysis of the thermal state of the base reveals large areas of a thawed bed and high melt rates at the interior of the GrIS (Fahnestock, 2001; MacGregor et al., 2016; Jordan et al., 2018). However, the ice surface motion response to the basal conditions can vary on several time scales (Ryser et al., 2014).

In Greenland, one feature causing the most significant discrepancies between numerically modelled and observed ice surface velocities is the Northeast Greenland Ice Stream (NEGIS) (Aschwanden et al., 2016), which therefore represents one of the largest uncertainties for ice flow predictions. Several studies assessed the genesis as well as the positioning and geometry of the NEGIS in its onset region close to the ice divide (Fahnestock, 2001; Fahnestock et al., 1993; Joughin et al., 2001). The ice stream is constrained by its 400-km-long shear margins, and their locations at its onset region show no apparent indications for a topographic control (Holschuh et al., 2014; Franke et al., 2020b). Christianson et al. (2014) established an extended hypothesis on the initiation and development of the NEGIS based on these studies and an analysis of data from an extensive geophysical survey at the onset of the ice stream, centred at the drill site of the EGRIP ice core where the ice stream widens (Vallelonga et al., 2014). The ice stream is most likely initiated by anomalous high geothermal heat flux (GHF) close to the ice divide (Fahnestock, 2001). The GHF is the primary control on the generation of basal meltwater and the sensitivity of the hydrology system (Smith-Johnsen et al., 2020). The subsequent production and distribution of basal water probably play a crucial role in the extent and positioning of the shear margins (Christianson et al., 2014). The increasing ice flow velocity of the onset of the NEGIS in its current geometry would lead to the development a surface trough, which is not consistent with observations. Hence, the ice mass loss must be compensated by more ice flowing through the shear margins into the ice stream (Christianson et al., 2014). The positioning of the shear margins and therefore the size of the fast streaming flow area of the NEGIS is especially sensitive to changes in the subglacial hydrology (Perol et al., 2015) and subglacial erosion (Christianson et al., 2014).

In present ice-sheet models, the NEGIS is rendered by deriving the controlling factors of the basal conditions from ice surface velocities (Larour et al., 2014; Smith-Johnsen et al., 2019). Estimates of basal resistance are not well enough represented to accurately model geometry or the surface velocities of the ice stream, as our understanding of processes and conditions is still very limited. In this regard, the analysis of the basal roughness has become important for glacial geomorphological research and an increasingly accepted attribute to describe subglacial conditions and to derive a controlling factor for the dynamics of ice-sheets (Smith et al., 2013). Basal roughness parameters can thus help us to discriminate whether the ice is underlain by softer sediments or harder rock, to reveal traces of former ice dynamics, to constrain the thermal regime and identify potential processes

of subglacial erosion and deposition of sediments (Bingham and Siegert, 2009). At present, the roughness of the bed topography is typically analysed by spectral analysis of vertical and horizontal topography variations, based on the approaches of Shepard et al. (2001); Taylor et al. (2004) and Li et al. (2010). Many studies of ice-sheet dynamics use a roughness analysis for a subglacial landscape interpretation to distinguish between hard and soft bed types, erosion and redistribution of sediments as well as to derive paleo-basal conditions (Rippin et al., 2014). Basal roughness is also a key parameter for the ice-bed coupling (Hughes et al., 2011), to model basal sliding (Wilkens et al., 2015) as well as a parameter for subglacial hydrology studies (Meyer et al., 2018). In many studies, basal roughness shows a clear correlation to basal drag and ice sheet velocity (Smith et al., 2013). In radio-echo sounding measurements, the roughness of the subglacial topography on different scales also influences the scattering of reflected radar waves (Jordan et al., 2017) and thus, the reflectivity of the bed (Jacobel et al., 2010). Furthermore, the intensity and reflection pattern of the bed return informs us about the reflection properties of the base, thus complementing inferences made by the roughness parameter.

The majority of subglacial roughness studies in Antarctica focus on outlet glaciers (Bingham and Siegert, 2007, 2009; Diez et al., 2018; MacGregor et al., 2013; Rippin et al., 2006, 2011, 2014; Taylor et al., 2004) with only a few studies extending over large areas (e.g. Eisen et al. (2020) in East Antarctica). In a study to model the surface flow field of Pine Island Glacier, Wilkens et al. (2015) related basal sliding to a bed roughness parameter and were able to reproduce some essential flow features, like the location of the fast-flowing central stream and various tributaries. One of the first studies of basal roughness in Greenland was conducted by Layberry and Bamber (2001) using the residual bed elevation deviation to quantify basal roughness. An estimate of the basal roughness distribution based on a spectral approach for those part of GrIS covered by radio-echo sounding data was given by Rippin (2013). A recent study by Cooper et al. (2019) indicates different relationships between ice flow and basal roughness parameters. They conclude that in certain regions of slow ice flow, coinciding with low vertical roughness (i.e. smooth topography), a mechanism other than basal sliding must control ice flow. Stearns and van der Veen (2018) observed that bed friction, which should control basal sliding, does not control the rapid flow of a large number of glaciers in Greenland. Furthermore, the inverse correlation between basal roughness and ice-sheet flow velocity (slow-flowing areas are mostly smooth, while increased ice flow shows rougher beds) encouraged the authors of more recent studies to rethink the influence of basal roughness to basal traction (Rippin, 2013). Possible mechanisms could be the thermal state at the base, subglacial hydrology and the rates of erosion and deformation of sediments. However, detailed studies of the basal conditions of glaciers and ice streams in Greenland have so far concentrated on a land-terminating section of the GrIS (Lindbäck and Pettersson, 2015). For Greenland, for instance, Cooper et al. (2019) discuss a more diverse relationship between basal roughness and its relationship with ice flow velocity and direction than evident from previous, more localised work.

In this paper, we use airborne radar data from AWI's ultra-wideband radar system to analyse the basal conditions of the onset of the NEGIS. We perform a spectral roughness analysis to characterise the pattern of the bed return signals and investigate the subglacial topography parallel and perpendicular to ice flow. For the basal roughness analysis on finer spatial scales, we analyse the radar reflections pattern from the bed return echoes. Based on an improved bed elevation model, we investigate subglacial water pathways. We then combine these data with the return power of the bed echoes to estimate where the temperate conditions prevail at the bed and liquid water is likely

to be present. By combining these approaches, we can better constrain the basal thermal regime than with either method alone. This should ultimately give a consistent picture of the processes at the base, which controls ice flow dynamics. Finally, we use our larger-scale data set to discuss the extended hypothesis of Christianson et al. (2014) of the initiation and development of the NEGIS as well as the positioning of the shear margins in its onset region.

Our results reveal a regional change in basal roughness and the pattern and intensity of the basal return echo from the upstream towards the downstream part in our study area on the NEGIS. Furthermore, we detect a bed roughness anisotropy concerning the ice flow direction, indicating streamlining parallel to ice flow. The analysis of water flow paths and the basal return power distribution supports the hypothesis that the subglacial hydrology mostly controls the position of the shear margins.

Data and Methods

Survey area and data acquisition

We use airborne radar data of the EGRIP-NOR-2018 survey in the onset area of the NEGIS (Figure 1). The data were collected with the AWI multi-channel ultra-wideband (UWB) airborne radar sounder (for details see Hale et al. (2016); Arnold et al. (2019); Franke et al. (2020b)) and recorded at a centre frequency of 195 MHz and a bandwidth of 30 MHz. A complete methodological description of the radar data processing and uncertainty estimation is described in Franke et al. (2020b). In the study area, the NEGIS accelerates from $\sim$10 to 80 m/a over a distance of roughly 300 km and widens from $\sim$20 km in the upstream boundary of our survey area to $\sim$65 km further downstream (Figure 1). More than 8000 km of survey profiles are distributed over an area of more than 250 km along ice flow direction and 50 to 100 km across, covering the interior of the ice stream, the shear margins and the slow-flowing area in the vicinity of the NEGIS (Figure 1). The profile spacing of across-flow profiles is 5 km in the central part of the survey area, near the drill site of the East Greenland Ice-core Project (EGRIP; `http://eastgrip.org`), and 10 km further upstream and downstream. Along-flow profiles are mostly aligned along calculated pathways of ice flow based on the velocity field of Joughin et al. (2017). For the rest of this paper, we will refer to upstream and downstream as the regions upstream and downstream of the EGRIP drill site, respectively.

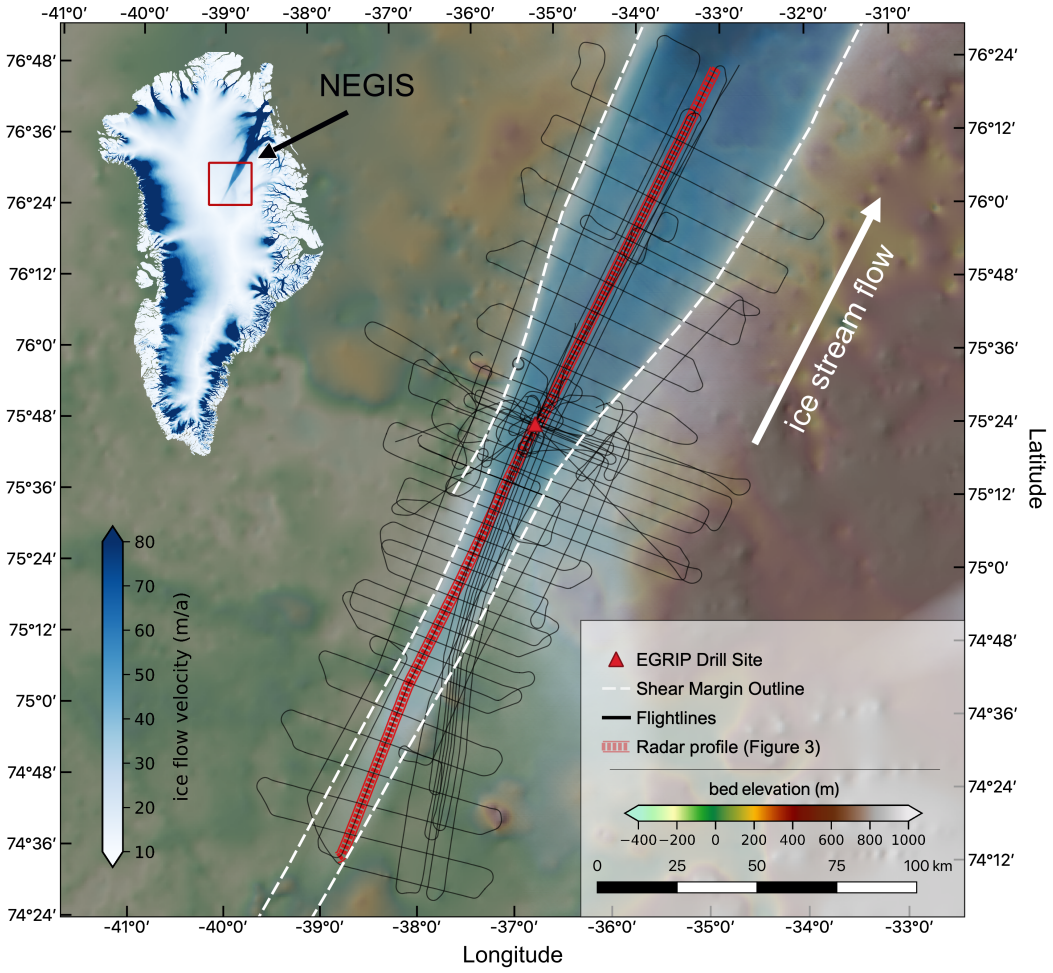

Figure 1: Overview of the survey area in the interior of the Greenland Ice Sheet at the onset of fast flow of the NEGIS. The black lines, which are centred at the EGRIP drill site, represent the survey profiles of the EGRIP-NOR-2018 airborne UWB radar survey (Franke et al., 2020b). The white dashed lines show the outline of the shear margins and the dashed red line the radar profile shown in Figure 3. Bed elevation is referenced to mean sea level (EIGEN-6C4 geoid (Förste et al., 2007), this reference applies to all other maps showing the bed elevation) and ice flow velocity is based on the dataset of Joughin et al. (2017) and is shown in blue colour code for velocities larger than 10 m/a. This map and all following maps are shown in the coordinate system EPSG 3413 (WGS84 / NSIDC Sea Ice Polar Stereographic North).

Basal Roughness Calculation

Assessing the roughness of the subglacial topography is important for characterising the topographic structure at different scales. We define basal roughness as the relative vertical and horizontal variation of the topography of the ice-bed interface. In our analysis we calculate three parameters (ξ, ξ_{sl} and η), which are commonly used to characterize basal roughness (Li et al., 2010; Gudlaugsson et al., 2013; Rippin et al., 2014; Cooper et al., 2019):

- ξ reflects the vertical irregularity of the bed and provides information about the dominating vertical amplitudes. This roughness parameter is defined as the integral of the wavelength spectrum over the range of a moving window (MW). Values close to 0 reflect the dominance of smaller amplitudes and a smoother topography.
- Wright et al. (2012) suggested to also use the vertical slope roughness ξ_{sl}, instead of just analysing the vertical amplitude, which acts as a filter and also indicates small-scale variations of vertical elevation changes.
- Li et al. (2010) introduced the frequency roughness parameter η, which is calculated by dividing the vertical roughness ξ by the roughness of the bed slope ξ_{sl}. This parameter reflects the horizontal variation pointing out the dominance of a particular wavelength. High values represent the dominance of longer wavelength and smaller values the dominance of shorter wavelength.

We use the bed picks of the EGRIP-NOR-18 data set (Franke et al., 2019, 2020b) for basal roughness calculation. The roughness analysis in this paper is based on the approaches of Hubbard et al. (2000) and Taylor et al. (2004) and uses a Fast Fourier Transform (FFT) to analyse the wavelength spectra of variations in topography (Gudlaugsson et al., 2013). This requires a uniform sampling interval of data points on the bed elevation profiles. Synthetic Aperture Radar processing of our radar data already includes the creation of a new coordinate system with a constant spatial sampling interval for the focused radar data. The average spacing between data points is 14.78 m. For each data point on a linearly detrended profile, we calculate the wavelength spectrum over a MW of 2^N data points. We test two different MW for our analysis: (i) $\sim$400 meters, which corresponds to 32 data points (N=5) and (ii) $\sim$2000 m, which corresponds to 128 data points (N=7). As pointed out by Taylor et al. (2004) and Rippin et al. (2014), 32 data points (N=5) is the minimum value that should be used. It is an appropriate MW length to study small-scale variations in the bed and to detect changes in basal roughness over a short distance. For this 32-data point MW, one data point covers the roughness at a resolution which is finer than the cell size of 500 m used for the bed elevation data sets of Morlighem et al. (2017) for Greenland and the NEGIS onset region by Franke et al. (2020b). To make sure that this small MW does not suppress long-wave structures, we compared the result of the 500 m MW with the results obtained for the $\sim$2000 m MW. The comparison shows that significant changes are represented in both MWs. Because we focus on regions where clusters of high or low roughness values or trends appear, we use the larger (N=7) MW for further analysis . For this manuscript, we will refer to this kind of basal roughness as *large-scale* roughness.

Because the interpretation of roughness parameters is highly directionally dependent and the dominating factor influencing bed formations as shown by Falcini et al. (2018); Gudlaugsson et al. (2013) and Rippin et al. (2014), we separately analyse along- and across-flow profiles. We present roughness values on a logarithmic scale to emphasize the range of up to four orders of magnitude. A comparison of ξ and ξ_{sl} shows that dominance of high vertical amplitudes correlates with steep slopes, which suggests that small amplitude vertical roughness values are not filtered. For further analysis, we therefore, excluded the slope of the vertical roughness ξ_{sl}.

Basal return power

We use the intensity of the return echoes from the basal interface as an additional parameter to analyse the basal conditions at the onset region of the NEGS. We follow the approach of Jordan et al. (2016) and Jordan et al. (2017), which is based on the method developed by Oswald and Gogineni (2008) and Oswald and Gogineni (2012). The return power is calculated from an along-track average of the basal return echo and is defined as the integral over a window of samples that represent the reflected energy from the bed (equation 1). Before arithmetically averaging along-track, we use the bed picks of Franke et al. (2020b) to shift the bed reflection to a single level. The arithmetical averages are phase-incoherent, but help to reduce fading effects and to smooth power fluctuations (Oswald and Gogineni, 2008). We tested different values for along-track averaging and found a good agreement with a constant value of 50 (two times 25 adjacent traces). The size of the range window is kept variable and is set for a threshold above 3.5% the noise floor for a section above the bed reflection (for further details, see Figure 3 in Jordan et al. (2016)). We follow Jordan et al. (2016) and define the integrated power P_{int}, referred to as the bed return power (BRP), by

$$P_{int} = \int_{Lupper}^{L_{lower}} P(L_i), \tag{1}$$

with the upper and lower limit of the integration window threshold L_{upper} and L_{lower}, the return power of a sample P and the depth range index L_i. The full waveform of the basal return in the integration window represents an overlay of the secularly reflected energy from nadir and scattered energy from along- and cross-track off-nadir (Young et al., 2016). The majority of the scatter from off-nadir will arise from across-track reflections because SAR post-processing reduces the footprint of return signals in along-track (Raney, 1998). Similar to the approaches of Jordan et al. (2016) and Jordan et al. (2018), we implement additional quality control rules. Traces where the window for the integration of depth-range bins was smaller than five range bins were abnormally thin and abrupt reflections associated with clutter and were removed. The maximum size of the integration window is set to 40 range bins to limit the amount of far off-nadir layover signals.

Radar wave bed return power is corrected for spherical spreading and therefore depends mainly on the properties of the ice-bed interface, scattering properties of the bed, anisotropy in the ice fabric and dielectric attenuation within the ice column. The largest energy loss is related to dielectric attenuation, which depends on ice temperature, chemistry and other impurities in the ice column (Corr et al., 1993; Matsuoka, 2011). If dielectric attenuation varies significantly, the distinction between basal water and dry sediment is difficult because the effect of englacial attenuation can be much more significant than the contrast in reflectivity between a wet and dry base (Matsuoka, 2011).

Waveform abruptness

The intensity of the integrated bed return echo as well as the length of the integration window is sensitive to small-scale variations in basal roughness (Cooper et al., 2019), which are not resolved in the radargrams and depend on the size of the Fresnel zone. The diameter of the Fresnel Zone for a bandwidth of 180—210 MHz and an ice thickness range of 2—3 km is $\sim$60 m. Surface roughness and the wavelength of the radar signal determines the nature of the electromagnetic scattering.

However, rough subglacial terrain can produce side reflections, which are difficult to separate from the nadir bed echo return. In this case, the footprint of the radar signal and consequently the area of the basal backscatter is larger as the Fresnel zone and determined by the beam angle of the transmitted signal. To characterize the basal scattering, we follow the approach of Oswald and Gogineni (2008) which has been adapted and extensively used in Greenland by Cooper et al. (2019); Jordan et al. (2016, 2017) and Jordan et al. (2018) analysing the waveform abruptness of the bed reflection. We follow Cooper et al. (2019) and define the abruptness parameter A by

$$A = \frac{P_{max}}{P_{agg}}, \tag{2}$$

where P_{max} is the maximum amplitude of the basal return echo in the integration window and P_{agg} the integrated basal return power (Oswald and Gogineni, 2008). A large P_{max} in a small integration window will result in a large value of A. If the reflected energy is distributed over a larger integration window, it will decrease the maximum amplitude and result in a small value of A (for details see Figure 4 in Cooper et al. (2019)). Hence, high values tentatively indicate the dominance of a specular reflector and lower values indicate either the dominance of a diffuse reflector (which corresponds to vertical roughness in along-track) or that the nadir reflection is overlaid by off-nadir reflections in the integration window (vertical roughness in cross-track). We will refer to this scattering-derived roughness as *small-scale* roughness because it represents roughness of a different scale and type than the spectral *large-scale* roughness.

Basal water routing

We compute (potential) subglacial water pathways from the hydrological potential F. We assume that the water flow depends on the elevation potential and the water pressure r_w (Shreve, 1972). Under the assumption of equilibrium between water pressure and ice pressure we can write

$$\Phi = \rho_w g b + \rho_i g H, \tag{3}$$

where ρ_w is the density of water, g is the acceleration due to gravity, b is the height of the ice base and H the ice thickness (Le Brocq et al., 2009; Livingstone et al., 2013). We apply a simple flux routing scheme as described by Le Brocq et al. (2006) to successively compute the number of upstream cells (cells that potentially contribute water to this cell) for each grid cell. The equilibrium assumption in equation 3 is only valid at large scales (km) and makes the potential especially sensitive to the ice surface gradient. Hence, this method cannot account for localised water flow in, e.g. channels (more details on our implementation can be found in Calov et al. (2018). We make use of bed topography and ice thickness data of the EGRIP-NOR-2018 bed elevation model from Franke et al. (2020b) as well as the BedMachine v3 topography (Morlighem et al. (2017); BMv3). We use both models as input fields to analyse the sensitivity of subglacial water routing to the bed topography. While this method allows for using basal melt rates as input to quantify transported water volumes, we chose to simply count the number of upstream cells as a measure for potential water pathways. Basal melt rates are poorly constrained for this area, in particular, because the spatial variations in geothermal heat flux are subject to considerable uncertainties (Jordan et al., 2018; Smith-Johnsen et al., 2019). Nevertheless, we can use the water pathways to estimate

the distribution of basal water, particularly for areas where we can infer a thawed base and the generation of meltwater by other methods. Several studies have detected or modelled water at the base, but the amount of basal water is uncertain and difficult to measure (Fahnestock, 2001; MacGregor et al., 2016; Jordan et al., 2018).

Results

Spatial distribution of spectral basal roughness

We analysed $\sim$370,000 data points for vertical and horizontal roughness with a spectral analysis approach and present our result as the dominating vertical amplitude (ξ) and horizontal wavelength (η) over a 2 km MW in along-flow and across-flow profiles in Figure 2. We observe that high ξ, in general, correlate with higher η values. Also, the cross-correlation of ξ and η shows higher vertical roughness values for the same horizontal roughness in cross-flow profiles compared to along-flow profiles. On the linear scale, vertical roughness values vary on the order of four magnitudes and horizontal roughness in the order of 2.5. Both basal roughness values and not making a distinction between along- and across-flow profiles show distinctly different spatial distributions in two areas: upstream and downstream of the EGRIP drill site (Figure 2). We will refer to these two regions as R_{up} (upstream) and R_{down} (downstream), respectively, and will present their particular characteristics in the following.

Region R_{up} shows low vertical and horizontal roughness values for profiles along- and across-flow. On average, ξ and η are small for profiles along-flow in the ice stream, while we observe an increase of ξ for profiles perpendicular to flow when moving from the upstream end in the south-west towards the EGRIP drill site. Across-flow profiles show distinctly different roughness values within and outside of the ice stream. Outside of the south-eastern shear margin, η is higher than inside the ice stream. Along-flow profiles that are located outside of the ice stream show similar horizontal and vertical roughness values as along-flow profiles in the ice stream. The transition zone between regions R_{up} and R_{down} is characterised by a dominance of lower vertical amplitudes (ξ) and shorter horizontal wavelengths (η). The statistical distribution of roughness values for both, ξ and η, for across-flow profiles is much wider. However, it has to be noted that the profiles also extend further to the South-East and North-West here than further upstream.

The bed elevation in the transition area rises about 500 m in flow direction and the average ice thickness decreases compared to the region R_{up}. Both, the vertical and horizontal roughness values, are on average higher for along and across flow profiles in the downstream region R_{down} in comparison to the upstream region R_{up}. Along-flow profiles show a strong increase in ξ and η, and both remain high in value with little variability. Along-track profiles perpendicular to ice flow, ξ shows a trend towards increasing values downstream and at the upstream end of region R_{down}. The horizontal roughness η shows two different domains for across-flow profiles. Low values of horizontal roughness dominate in the south-eastern part of region R_{down}, which we will refer to as region R_{east}, and high values in the north-western region R_{west} (Figure 2d). The transition from high to low values between these two subregions, which we will refer to as R_{trough} (Figure 2c), coincides with the steep eastern flank of a central ridge as well as with a local topographic low (Franke et al., 2020b). In the region R_{trough} we observe low vertical roughness values in the centre and higher roughness values at the edges of the region. For region R_{down}, along-flow profiles located outside

of the ice stream, show a similar development in both, ξ and η (Figure 2a and b). For the parts of across-flow profiles, which are located outside of the shear margin, we detect the same trend of increasing vertical roughness from upstream to downstream (Figure 2c), but not in horizontal roughness because it shows greater variability at across-flow profiles (e.g. the difference in η in the regions R_{east} and R_{west} in Figure 2d).

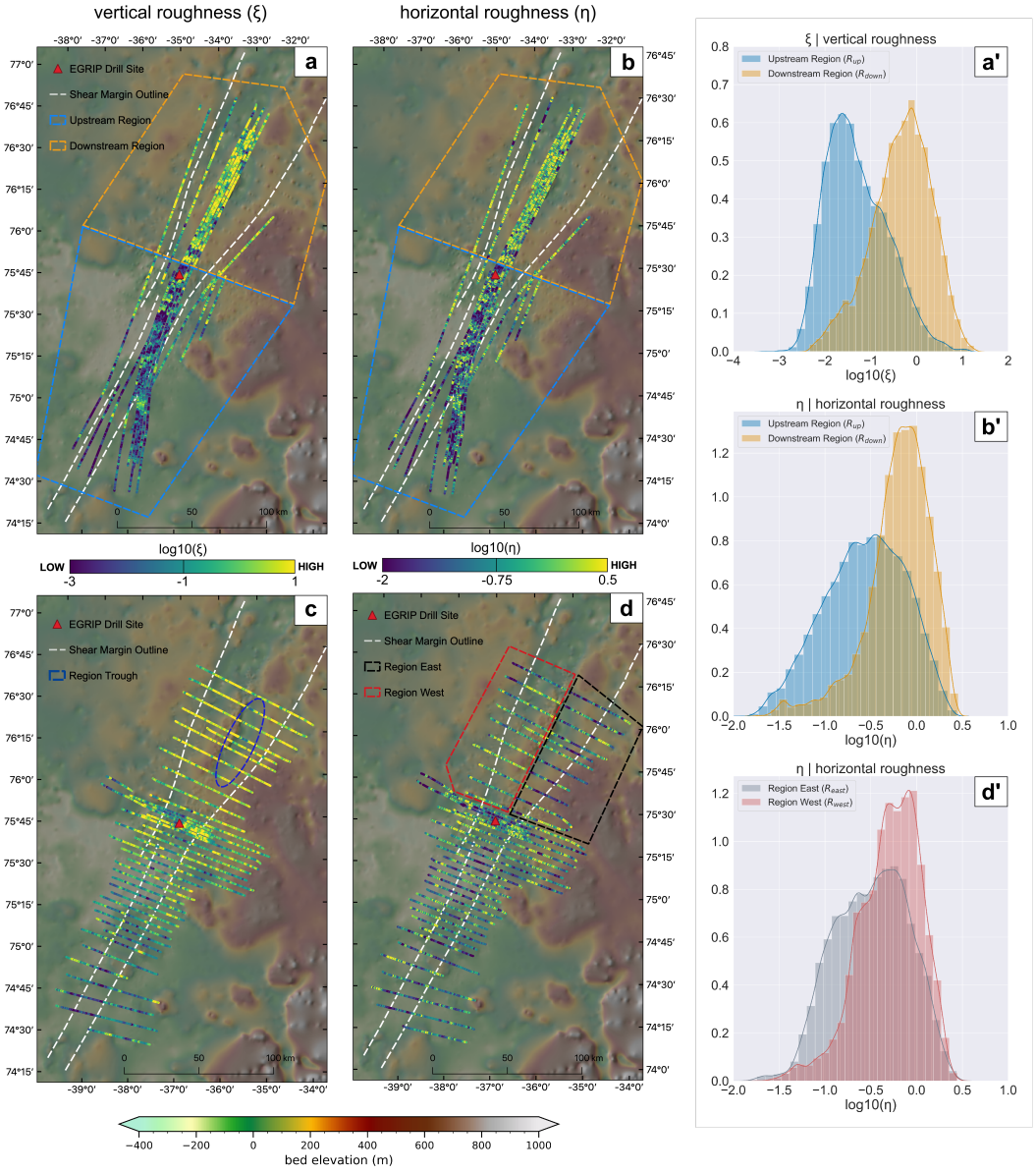

Figure 2: Survey area at the NEGIS showing (a) along- and (c) across-flow profiles of the vertical roughness parameter ξ and the horizontal roughness parameter η in (b) along and (d) across-flow profiles respectively. Both parameters are shown on a logarithmic scale. The background map represents the EGRIP-NOR-2018 bed topography of Franke et al. (2020b) in meters, referenced to mean sea-level (EIGEN-6C4 geoid). Histograms a' and b' show the distribution of ξ and η for the along-flow profiles for the upstream and downstream region, respectively (orange and blue outline in a and b). The y-axis on the histograms represents the kernel density estimation. The distribution of η in the western and eastern part of the downstream region (red and black outline in d) are shown in a histogram d'.

Development of ice stream flux in a geometrical context

Figure 3a shows a radargram oriented along-flow at the location indicated in Figure 1and 4 with a red line. This radar section is composed of two profiles and was concatenated at the location of the EGRIP drill site. The profile from 0 to 160 km will be referred to as the upstream section and the profile from 160 to 280 km as the downstream section. There is an offset between the two profiles of 1 km across-flow. For both sections, we tracked two internal reflection horizons, which have a respective age of $\sim$30 and 52 ka, respectively, which we transferred from dating of radar reflections at the location of the NGRIP ice core (Vallelonga et al., 2014). We will refer to the thickness of these two layers as the basal unit between the 52 ka horizon and the bed reflection; and the internal unit between the 30 ka horizon and the 52 ka horizon, respectively. The upstream section shows an increase of ice surface velocity (Figure 3b) from 12 to 58 m/a over a distance of 150 km. Vertical and horizontal roughness (Figure 3c and d) are on average low but vary over two to three orders of magnitude. Furthermore, the thickness of the internal and basal unit remains nearly constant in the upstream section (Figure 3e). In the downstream section, between 150 and 175 km, we observe a decrease of the internal unit thickness, whereas the basal unit thickness remains constant downstream to 240 km. The surface velocity in the downstream section shows a small decrease between 175 and 210 km and increases thereafter to $\sim$80 m/a. Vertical and horizontal roughness in the downstream section is higher on average than in the upstream section. The increase in roughness correlates with a decrease in ice surface velocity and also with a decrease in the thickness of the ice column. The internal unit becomes thinner while the thickness of the basal unit remains constant.

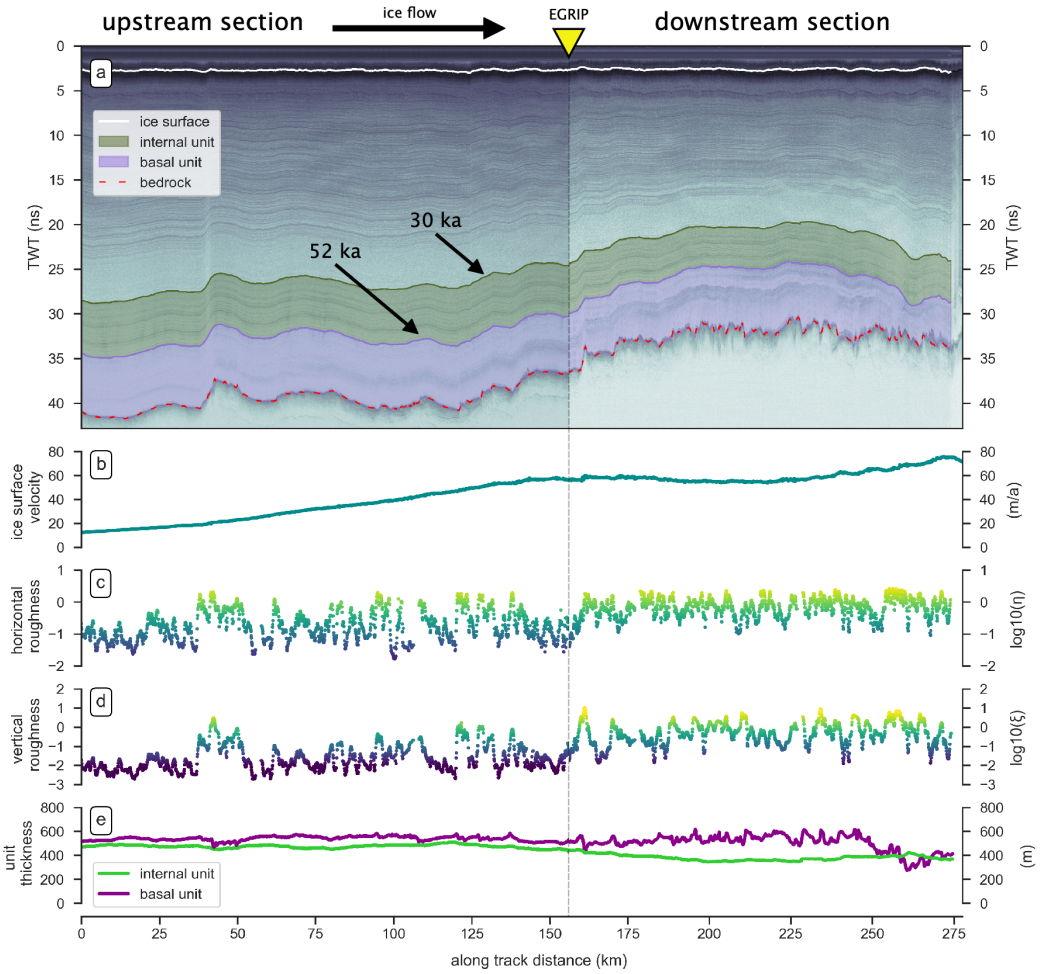

Figure 3: Evolution of several basal and englacial properties in ice flow direction, extending from far upstream to the downstream end of our survey area (red line in Figure 1 and 4). Because there is no continuous survey profile, the downstream part (right part of the dashed line) is offset $\sim$1 km to the South-East (transverse to along-flow profile orientation) relative to the upstream profile (left of the dashed line). The transition between the two profiles marks the position of the EGRIP drill site (yellow triangle). Ice flow direction is from left to right. (a) along-flow radargrams with continuously tracked surface (white), two internal ice units (basal unit in purple and internal unit in green) and bed reflection (red dashed line); (b) ice surface flow velocity; (c) horizontal roughness η and (d) vertical roughness ξ, both with the same colour code and scaling as in Figure 2; and (e) the thickness of the internal and basal unit.

Figure 4 shows the downstream section and the spatial distribution of ice surface velocity, flow lines indicating the flow path (Figure 4a) of a point on the ice surface, as well as vertical and horizontal roughness (Figure 4b and c respectively). Surface flow velocity is about 5-8 m/a higher in the eastern part of the section as in the western part. The area of increased ice surface velocity correlates with the location of the basal topographic depression (R_{trough}) and is also characterised

by lower vertical and horizontal roughness. Flowlines in Figure 4a show that ice surface flow in the eastern part of the region (yellow flow line in Figure 4a) deviates slightly towards south-east (orographic right) as it flows around the central ridge trough the topographic depression, whereas a flowline located north-west to the ridge bend less towards the trough (green flow line in Figure 4a).

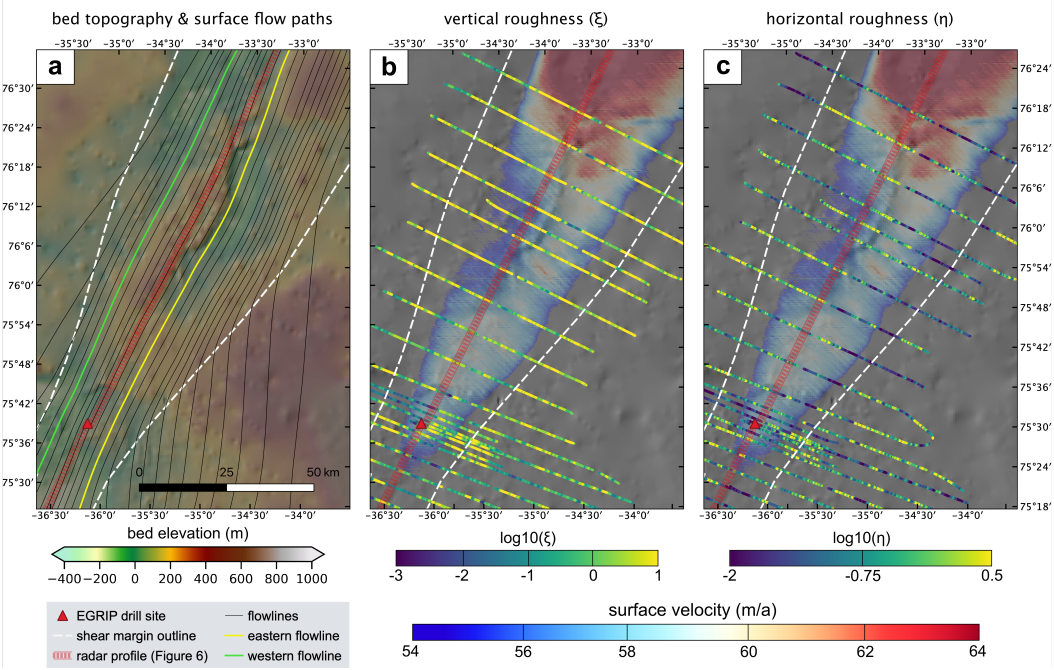

Figure 4: Bed and flow properties in the downstream survey region, North-East of the EGRIP drill site (red triangle). Panel a shows the bed topography and flowlines of the ice surface (ice flow direction is towards North-East as indicated in Figure 1). Panel b shows the vertical roughness parameter ξ as well as the ice surface velocity (Joughin et al., 2017) in a range of 54 to 64 m/a (velocity values lower than 54 m/a are transparent). Panel c shows the same velocity map together with the horizontal roughness η. Both roughness maps (b and c) show the hillshade of the bed elevation in the background. The red line on all three maps represents the location of the radar profile in Figure 3.

Basal return power and waveform abruptness

In Figure 5 we present the BRPof the basal reflection in (dB) for profiles aligned along-flow (a) and across-flow (b). The basal return power, which is corrected for spherical spreading, varies in a range of -67 to -20 dB and is on average higher in the downstream region R_{down} than in the upstream region R_{up}.

The BRP for the area around the EGRIP drill site agrees with the data of Christianson et al. (2014) and (Holschuh et al., 2014). These two studies analysed the BRP in the immediate surrounding of the EGRIP drill site, which they characterised as high return power in the centre of the ice stream, low return power in the area of the shear margins and again higher return power outside of the shear margins. In the upstream region, the BRP is distributed unevenly inside and outside of the

ice stream. In general, the BRP on along- and across-flow profiles within the ice stream is higher than outside. Larger values on across-flow profiles in the upstream region are concentrated in a $\sim$10 km corridor in the middle of the ice stream and show highest values in the centre and an overall decrease towards the shear margins. Along-flow profiles inside of the ice stream show a stronger BRP than profiles located outside of the ice stream. Downstream of the EGRIP drill site, where the ice stream is widening, high return power values are not constrained to the centre of the ice stream. Along-flow profiles show a slightly higher variation than across-flow profiles. The strongest variations coincide with the location of the central ridge. In contrast to the pattern upstream, the high basal return power of across-flow profiles in R_{down} extend $\sim$5-20 km beyond the shear margins into the slower flowing areas. Furthermore, along-flow profiles located outside of the ice stream, show a similar high BRP as profiles inside.

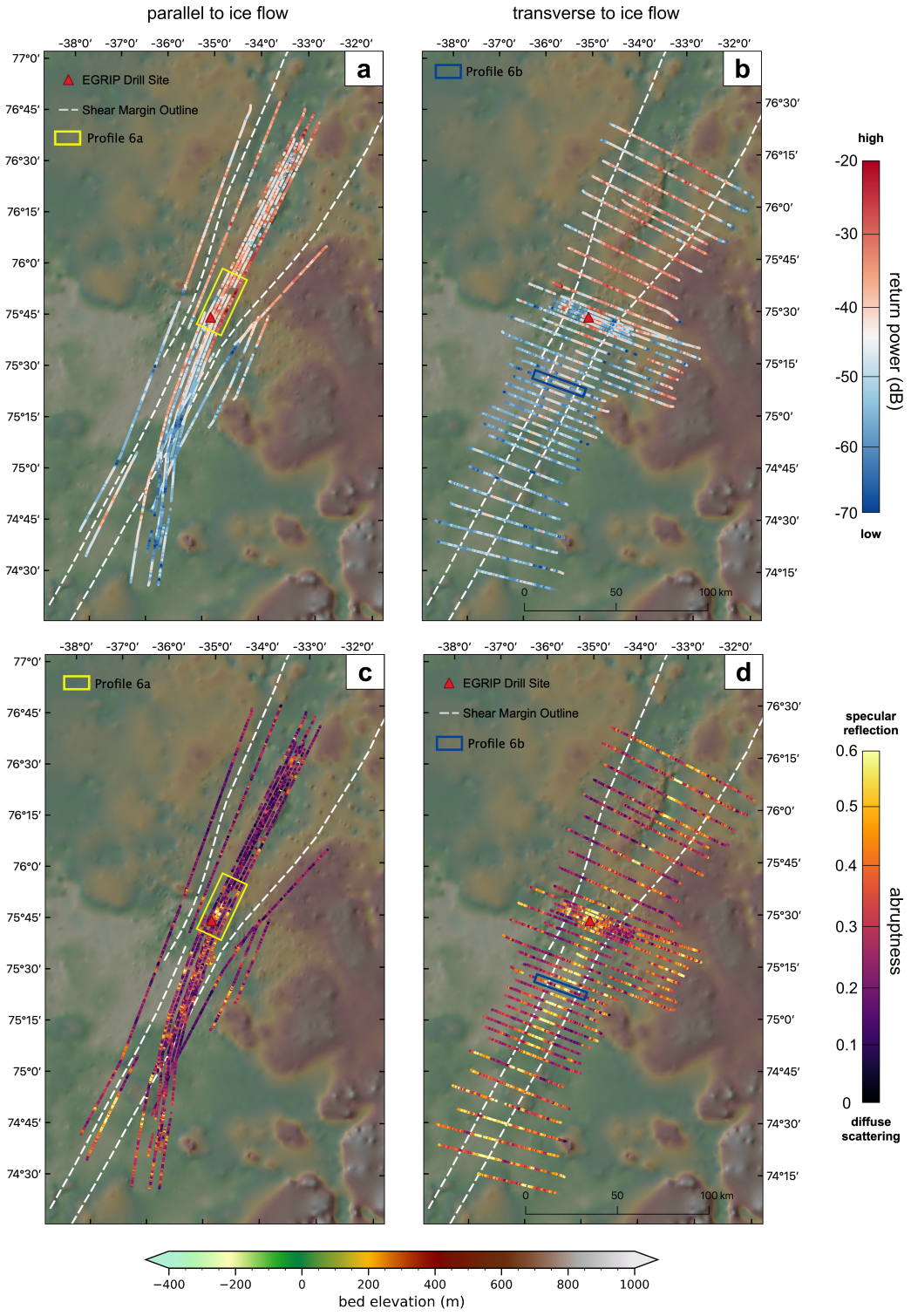

Figure 5: Bed echo characteristics for (a and b) basal return power and (c and d) waveform abruptness for profiles oriented along-flow (a and c) and across-flow (b and d), respectively. Basal return power is corrected for spherical spreading and displayed in decibel (dB with respect to unity). Waveform abruptness is expressed as the ratio between the maximum BRP and the integrated bed return power and is thus unitless. High values (yellow) represent the dominance of specular reflection and low values (dark purple) the dominance of diffuse scattering of the base. The yellow and blue rectangular outlines indicate the position of the radargrams in Figure 6.

Figure 5c and d show the spatial distribution of the waveform abruptness for along- and across-flow profiles, respectively. Abruptness values range from 0.03 to 0.6, where smaller values are associated with a dominance of diffuse scattering and higher values with more specular reflections. Along-flow profiles show significantly lower average abruptness values than profiles oriented vertically to ice flow in both, the upstream and downstream region. Furthermore, along-flow profiles in the upstream region show slightly higher abruptness values than the downstream region. Across-flow profiles in Figure 5d show the highest values in the upstream survey area, which are concentrated in the centre of the ice stream. This patch of high abruptness values has a similar extent as the patch of high basal return power in Figure 5b. Lower abruptness values in the upstream area are aligned in a zone extending 2-5 km from the shear margin to the ice stream centre and outside of the shear zones. In the downstream area, high abruptness values are located in a zone of a localised topographic depression (R_{trough}) as well as in the immediate surrounding of the EGRIP drill site. Abruptness values in the downstream region, outside of these two areas are significantly lower.

Two representative radargrams for the upstream and downstream region with their corresponding bed return power and abruptness are shown in Figure 6. An across-flow profile from the upstream section (Figure 6a) is indicated with the blue outline in Figure 5b and d and an along-flow profile of the transition zone from the upstream to the downstream region is located in the centre of the yellow outline in Figure 5a and c. Profile 6a shows high bed return power and high abruptness in the centre of the ice stream (outlined with the black dashed line) and outside of the ice stream close to the shear margin (white and grey dashed line). The along-flow Profile 6b shows on average a constant high basal return power. The waveform abruptness is on average higher between 0-12 km along-track and decreases thereafter. This change correlates with a step in the bed elevation, which marks a general change of the topographic regime.

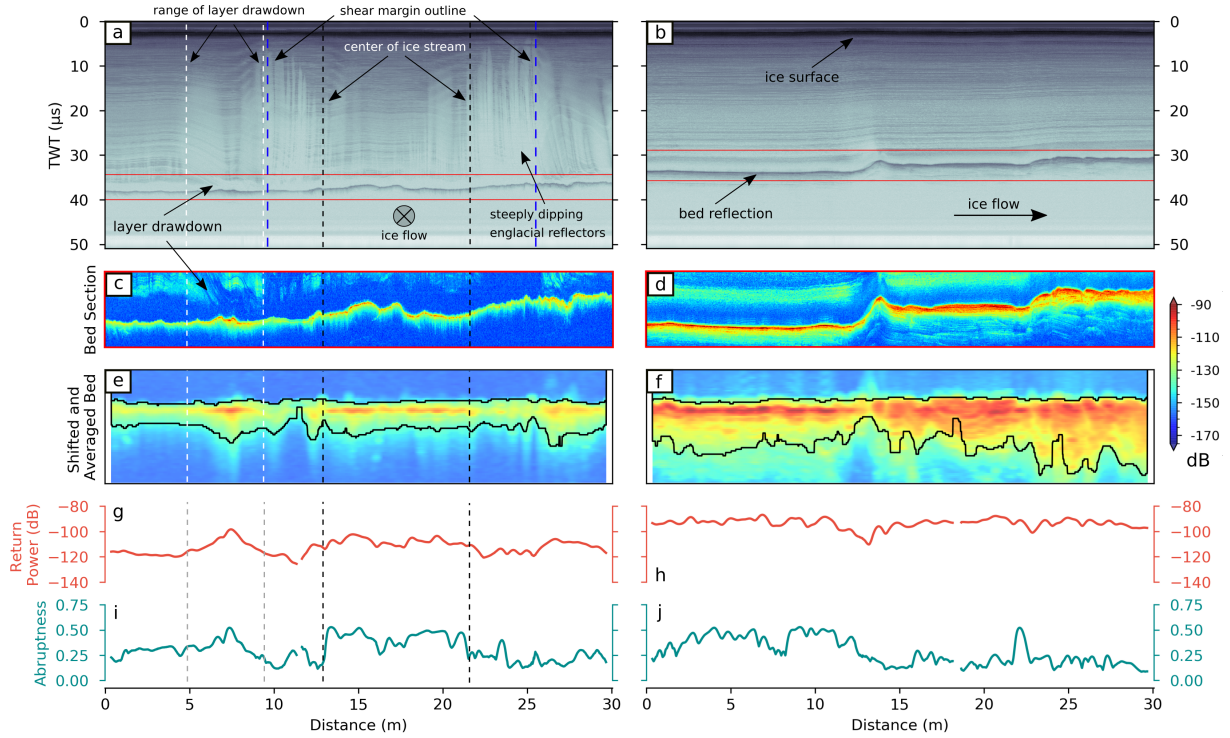

Figure 6: Two radar sections (two-way travel time (TWT) on the y-axis) and basal return echo properties from (a) an across-flow profile (location is indicated in Figure 5b and d with the blue outline) and (b) an along-flow profile (location is indicated in Figure 5a and c with the yellow outline). Panels c and d represent the analysis window of the ice-bed interface of the corresponding radargrams (indicated with the red lines in the radargrams) and their amplitude in dB, which are not corrected for spherical spreading. Panels e and f show the elevation-levelled basal reflectors and the corresponding basal return power after along-track averaging. The black outline represents the window of integration for basal return power. Panels g and h show BRP corrected for spherical spreading and (i and j) the waveform abruptness. The white dashed lines show the region outside of the shear margin and the black dashed lines the central part of the ice stream.

Basal water routing

The subglacial water flux follows the gradient of the hydraulic potential. The direction of the water pathways is in general oriented towards the direction of ice flow downstream and decreasing ice thickness (Figure 7). We compared subglacial water routing derived by the EGRIP-NOR-2018 bed elevation model and the BMv3 bed elevation model (blue and red lines in Figure 7 respectively). The general pattern is the same: In the upstream region, pathways with the highest inflow lead into the ice stream and flow around bed obstacles. About 20 km upstream of the EGRIP drill site, the main water pathways lead through the shear margins into the ice stream towards the point of lowest bed elevation. The pathway with the highest number of upstream routing cells is entering the ice stream from the South-East. About 10 km upstream of the EGRIP drill site the routing inside of the ice stream follows the south-eastern shear margin and propagates downstream. Pathways entering

the ice stream at the north-western shear margin propagate along the shear margin downstream. At the location of the drill site, the ice stream widens from $\sim$25 km to $\sim$60 km at the downstream end of our survey area and two dominant pathways develop in the ice stream: One on the south-eastern side of the ice stream with a higher number of upstream cells, and a second on the western side of the NEGIS. About 40 km downstream of EGRIP, the south-eastern path changes its location from the eastern shear margin to the local trough (our subregion R_{trough}), continuing in ice-flow direction and then switching its location back to the shear margin after another 40 km. The north-western pathway stays more or less in the area of the shear margin. Summarizing, the water routing in the downstream area seems to predominantly follow the location of the shear margins and local troughs in the bed topography in the ice stream.

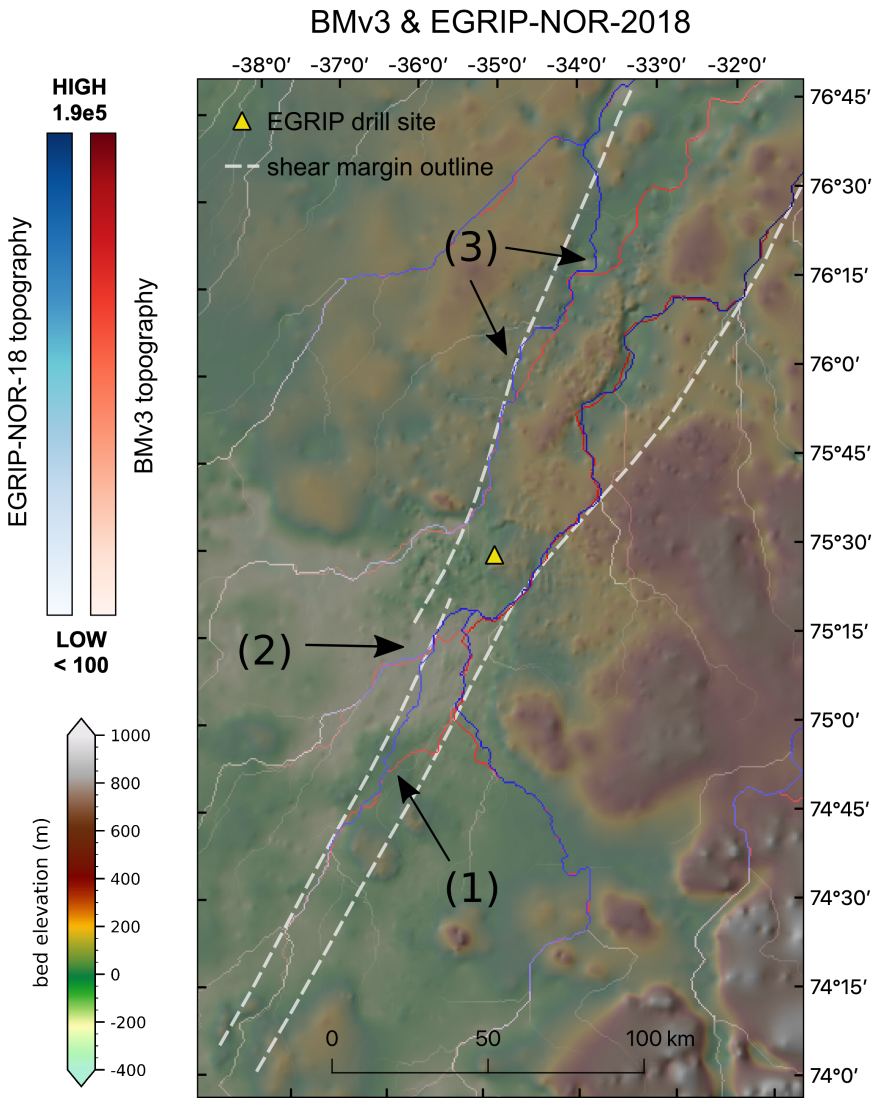

Figure 7: Basal water routing pathways calculated based on EGRIP-NOR-2018 bed elevation (Franke et al. (2020b); in blue) as well as pathways calculated with the bed elevation model BMv3 (Morlighem et al. (2017); in red). The basal water routing colour saturation represents the number of accumulated upstream cells. Pixels containing less than 100 upstream cells are transparent. High values and dark colours represent pathways that transport larger amounts of upstream cells. Features 1 – 3 present locations where the routing pathways from the two bed elevation models show the largest deviations. The background map represents the bed elevation of the EGRIP-NOR-18 data.

We identify three locations where the routing pathways deviate significantly for the two topographies (features 1-3 in Figure 7). At all three features, the blue EGRIP-NOR-2018 water routing follows preferably the location of the shear margin outline, whereas the BMv3 routing deviates and flows

430 towards the centre of the ice stream.

431

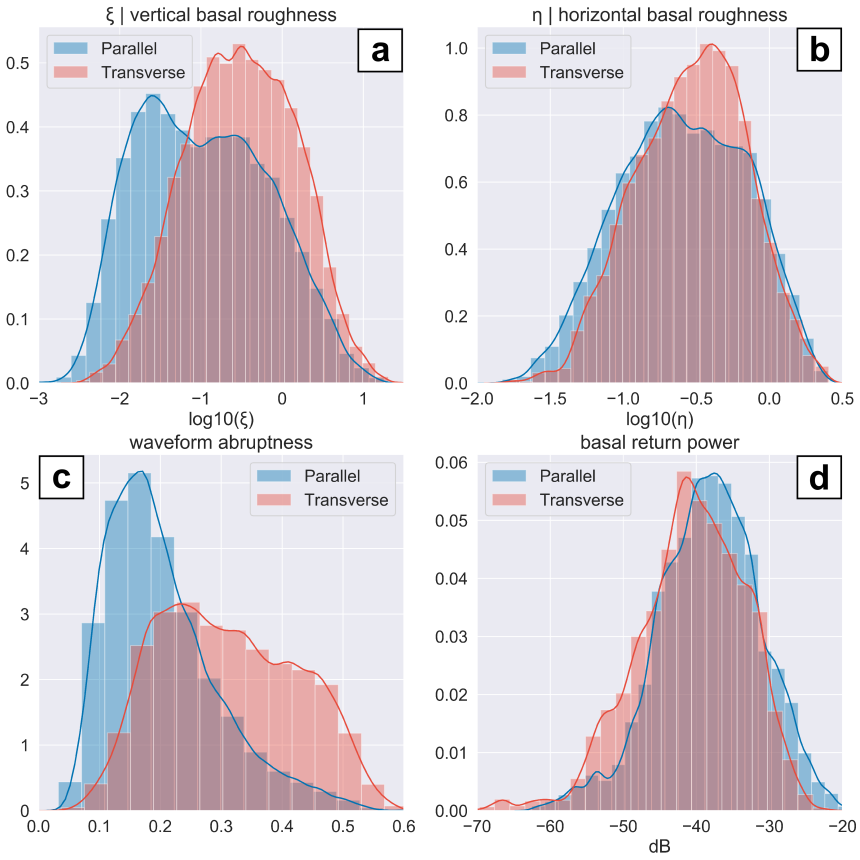

Figure 8: Histograms presenting the distribution of (a) vertical basal roughness, (b) horizontal basal roughness, (c) waveform abruptness and (d) basal return power for profiles oriented along- and across-flow for the location inside of the ice stream. Blue bins represent along- and red bins across-flow profiles. The y-axis shows the kernel density estimation.

432 Discussion

433 The analysis and interpretation of the conditions of the ice base inferred by airborne radar sounding
434 data are subject to several uncertainties resulting from radar data processing, the energy loss in
435 the ice column as well as the interpretation of basal roughness parameters. We address these
436 uncertainties in detail in the appendix.

437 Interpretation of large-scale basal conditions

438 The observation of higher *large-scale* vertical roughness values in the faster-flowing area of our study
439 region does not conform with the results of other roughness studies in West Antarctica (Bingham

and Siegert, 2009; Diez et al., 2018; Rippin et al., 2014; Siegert et al., 2005, 2016). These studies conclude that fast ice flow is mostly topographically controlled and associated with a smooth bed, while slow-flowing areas are characterised by a rougher bed and the absence of a trough. Rippin et al. (2011) suggest that a smooth bed hints to a decrease of basal drag, favouring high ice-flow velocities. In contrast to our study, those study areas were concentrated mostly on the terminating part of glaciers. Therefore, we cannot directly relate to the interpretations from studies investigating outlet glaciers and ice streams.

Because our region of interest is located in the interior of the GrIS near the onset region of NEGIS, where ice flow velocity increases from 10 to 80 m/a, our observations and inferred properties suggest that the smooth bed, which is probably temperate, facilitates ice-flow acceleration, in particular when liquid water is available at the base. Cooper et al. (2019) find several slow-flowing regions in Greenland. These are among them a sub-region of our survey area similar to our upstream region R_{up}.

The generally higher values of vertical roughness in across-flow profiles in comparison to along-flow profiles in the cross-correlation of ξ and η (Figure 8a and b) is an indication that the bed has been modified by ice flow. A higher ξ across-flow is very likely caused by streamlining of the bed in ice flow direction. In the upstream region R_{up}, we find a clear trend towards higher vertical roughness along flow inside of the ice stream. We interpret that increasing ice flow velocities enhance streamlining at the bed, which is supported by the observations of Franke et al. (2020b), who interpret off-nadir side reflections as an indication for the presence of elongated subglacial landforms in this part of the NEGIS.

Further downstream the ice stream slows down on its northern side due to a step in the bed topography and a general change of the terrain, which might be due to a change in bedrock type, and thus a higher mean vertical roughness, which is probably not related to ice flow. At this point the flux of ice into the ice stream probably cannot be compensated by acceleration, thus causing the stream to widen to increase downstream flux. In the upstream part, the low vertical roughness facilitates the acceleration of the ice stream, as the NEGIS can compensate the influx of ice through the shear margins and without changing its width.

In contrast to the large-scale roughness, the small-scale roughness is defined by the reflection pattern and energy distribution of the bed echo. The resolution of a single point can range from $\sim$60 m, which is the footprint of the Fresnel zone, to several 100s of meters if off-nadir side reflections interfere with the nadir return signal. For the analysis of the small-scale roughness, it is assumed that the energy reflected from a diffuse reflector in a large integration window should be proportional to the reflected energy of a specular target in a small window. The small-scale roughness is a measure for bed roughness in the across-track dimension of a radar profile. Low abruptness values indicate a rather diffuse reflection and high values a rather specular reflection transverse to the flight trajectory. If an intersection of two profiles shows a high value of A in an across-flow profile and a low A on an along-flow profile, we can infer a geomorphologic anisotropy, that indicates streamlining in ice flow direction (Figure 8c). This anisotropy is significant in the centre of the ice stream in the upstream region (Figure 5c and d) and supports the hypothesis of a streamlined bed.

In contrast to the pattern in the waveform abruptness, we find no significant directional anisotropy in basal return power (Figure 8d). The basal return power can be influenced either by the scattering characteristics of the base, englacial energy loss due to folded internal layers or scattering, the

thermal state of the ice as well as the availability and amount of liquid water at the base or a combination of these factors. Because there is no erosional trough, we do not observe significant changes in ice thickness between the ice stream and its surrounding.

Englacial attenuation should be higher in the ice stream than in the surrounding ice (Matsuoka et al., 2012) and probably highest at the shear margin due to an increase in ice temperature by internal shear. The temperate ice in the shear margins will probably have the largest effect on attenuation of the BRP for the entire survey region. The steeply dipping englacial reflectors, as indicated in Figure 6a, will, however, only reduce BRP in the shear margin area (Keisling et al., 2014) or other areas with pronounced internal deformation.

An explanation for the high BRP in the centre of region R_{up} could be interpreted as an indication for weak, porous, water saturated sediment, following similar interpretations of Rippin et al. (2011). Due to the subglacial routing system, water is continuously channelled towards the ice stream and weakens the subglacial sediments, which could have a potential stabilising effect on the ice flow (Bougamont et al., 2014). Our routing paths indicate that basal water does not leave the ice stream. Consequently, the base is increasingly lubricated, reducing basal shear stress and facilitating basal slip.

The analysis of basal water routing shows that in the downstream region the water is distributed towards the shear margins. This pattern is much more consistent in the routing scheme calculated with the new high-resolution EGRIP-NOR-2018 bed topography. This highlights the importance of high-resolution bed elevation models to determine the subglacial water routing accurately. The funnelling of water towards the shear margins could explain why basal return power in the shear zones is higher in the downstream part than further upstream. This supports the hypothesis that the geometry of the NEGIS is strongly influenced by the subglacial hydrology system (Perol et al., 2015). Only a few regions in our survey area would be candidates for a topographically controlled positioning of the shear margins. Basal water is distributed to both shear margins and propagates downstream without changing the general flow pattern along the shear margins. If the position of the shear margins is particularly sensitive to the subglacial water pathways, this could facilitate the ice stream at this position.

As the shear margins in the upstream regions of NEGIS appear not to be constrained by the bed topography or the basal substrate, their location might be fluctuating over time, allowing a more sensitive reaction to large-scale changes in the entire catchment area. Temporal variations in the surface slope of the ice sheet in Northeast Greenland, caused by changes in accumulation, distribution of surface melt or ocean forcing, can influence the subglacial water pathways Karlsson and Dahl-Jensen (2015). Hence, a warming climate with changes in the surface mass balance and characteristics in central Northeast Greenland may also influence the positioning of the shear margins of the NEGIS, or ice streaming in general.

Localised geomorphological and geological features

The abrupt increase of ξ and η in region R_{down} is probably associated with a change in lithology because the roughness change coincides with a general change of topographic terrain properties. Downstream of the EGRIP drill site, the bed elevation is higher and the topography much more variable than upstream. A difference in horizontal roughness of the eastern (R_{east}) and the western

region (R_{west}) of the downstream area (Figure 2d) as well as the local variations of vertical roughness in region R_{trough} (Figure 2c), could be explained by a different geomorphological setting. In this area, the interpretation scheme of Li et al. (2010) would explain the roughness distribution well. R_{east} shows a topographic depression and faster ice flow, low η and ξ indicate material which is easier to erode. The geomorphic interpretation for the western region R_{west}, showing higher η and ξ, could be a mountainous setting with minor erosion and deposition of sediments and slower ice flow (Li et al., 2010). A setting similar to the downstream area of our survey region can be found in Antarctic ice streams: a central ridge oriented along-flow, showing evidence for elongated subglacial landforms and indicating long term ice flow, and a several meters thick sediment. This has been reported for the Rutford ice stream (King et al., 2009) as well as Pine Island Glacier (Bingham et al., 2017; Brisbourne et al., 2017).

The increase of ξ along ice flow, the anisotropy of basal roughness, as well as the high waveform abruptness values in across-flow profiles within the ice stream in the upstream region R_{up}, indicate the development of elongated subglacial landforms inside of the ice stream. This is consistent with other observations (Christianson et al., 2014; Franke et al., 2020b). In several along-flow profiles on the central ridge in the downstream region $\mathrm{R_{down}}$, we observe a side reflection pattern beneath the bed reflection, indicating side reflections of along-flow oriented structures (for details see Franke et al. (2020b)). The pattern is similar to the bed striations found by Arnold et al. (2019), which are probably caused by glacier flow and suggest that elongated subglacial landforms are also present in this part of the survey area.

The appearance of elongated subglacial landforms can also occur at the shear margins of NEGIS, where Riverman et al. (2019) find flow parallel features composed of saturated, soft, high-porosity till. Elongated subglacial landforms like mega-scale glacial lineation can form on soft beds, but also on hard-beds, although the generation of hard bed streamlining probably takes more time or higher ice flow velocities (Krabbendam et al., 2016). Because the ice surface velocities at the location where we interpret elongated subglacial landforms are comparably low, we argue that these landforms were probably generated on a soft and deformable bed. This interpretation is also in agreement with the findings of unconsolidated sediments of Christianson et al. (2014). In the upstream region basal roughness patterns in along-flow profiles outside and inside the ice stream (Figure 2a and b) are similar, which indicates that the basal properties, and thus potentially basal substrate do not vary across the shear margins. Vallelonga et al. (2014) showed that sediments around the EGRIP drill site are present outside of the shear margin and suggested based on this findings, that the location of the shear margin could shift its location and maybe response to a rerouting of basal water.

In the downstream region we observe a decrease in acceleration of the ice stream. Higher average vertical roughness contribute to an increase basal resistance and a slope in the bed topography decreases the local driving stress in this region. Around the location of the EGRIP Camp, the ice stream is widening and the ice thickness is reducing by $\sim$700 m. The thinning appears not to be uniform over the entire ice column, as the lowermost ice layer, until 200 m above bedrock, does not change its thickness (Figure 3a and e). This could be interpreted as a transition in the stress regime from pure to simple shear at the base of the ice and thus less basal gliding. Indeed, a decrease in ice flow velocity can be observed at this location, which could be caused by a decrease in gliding. An increase of internal shear and deformation within the ice would also raise the enthalpy and enhance meltwater production, but additional water appears not to be compensating the effect of the enhanced roughness. The basal unit retains its thickness for more than 100 km further along

flow, which could be explained by decreased longitudinal stretching. This process would indicate an increased rate of internal deformation (Bons et al., 2018).

The drawdown of internal layers at the outer edges of the shear zone (e.g. Figure 6a) indicates high melt rates just outside of the ice stream. Thermomechanical modelling supports this finding and suggests that the shear margins are associated with the development of temperate ice condition near the bed, with temperatures exceeding the pressure melting point (Perol and Rice, 2015). Three-dimensional thermomechanical modelling suggests that fast ice flow in the centre of our survey region is facilitated in part by thermally softened ice at the shear margins. The dipping reflectors reduce the return power close to the shear margin in the upstream region. A difference between the up- and downstream regions could be explained by less basal water upstream, as the effect of the dipping reflectors should not be changing along flow. At the transition from R_{up} to R_{down}, basal return power is equally high in the centre of the ice stream as in the margin region and beyond, which points to greater amounts of basal water. The transition zone of these two patterns is characterised by spots of high basal return power located outside of the ice stream (see Figure 6a) at the onset of the shear margins (red dashed regions in Figure 9). A part of the water is probably produced at the shear margin itself, due to an increase of shear stress caused by the higher velocity gradient. This interpretation agrees with a subglacial hydrology modelling study by Riverman et al. (2019). They suggested that subglacial bedforms in the shear margins are created by melt out of sediment within the ice column. The share of power loss due to steeply dipping internal reflectors in the upstream and downstream region is probably in the same order of magnitude. Therefore, regardless of the attenuation caused by variations in impurity content, temperature or dipping reflectors, the increase of basal return power at the shear margins in the downstream region is most probably related to a change of reflectivity at the base and most likely by a higher amount of subglacial water.

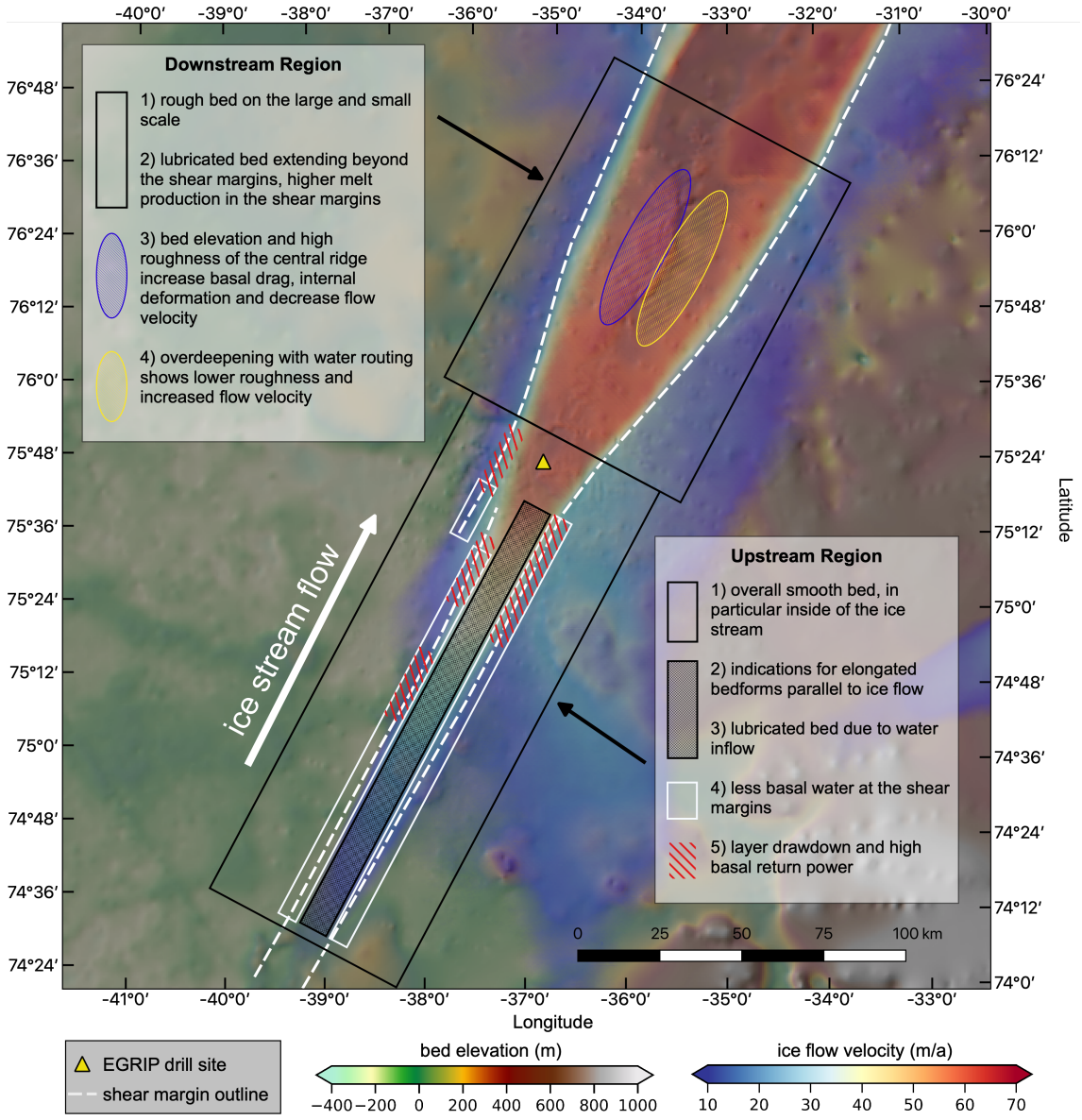

Figure 9: Summary of the basal properties of the (a) upstream and the (b) downstream survey region.

Synopsis of NEGIS characteristics

A summary of the key findings and interpretations for the basal conditions of the NEGIS in the onset region are presented in Figure 9. Our results support the hypothesis and mechanisms proposed by Christianson et al. (2014). In the onset region of NEGIS, available meltwater and the presence of a soft, deformable bed provide lower resistance for sliding and facilitate accelerated ice flow. Given increasing velocities in the upstream region, the soft bed is most likely strongly deformable, leading to longitudinal geomorphological bedforms. Decreasing ice thickness with faster ice flow

and higher basal melt rates change the hydraulic potential such that more water is routed into the ice stream from neighbouring areas. With increasing shear stress in the shear margins, additional water is produced by higher velocity gradients. Further downstream, where the ice stream widens, basal water is pushed towards and beyond the shear margin, partly because of the local topography and lithological properties, partly because of surface slopes of the ice surface. This leads to less resistant basal properties at the margins and enables a widening of the ice stream. Inside of the ice stream in the downstream area, basal shear stress is on average higher than upstream and the bed topography more variable. This produces non-uniform lateral ice surface velocities and an increase in the rate of internal deformation of the basal ice unit.

Conclusions

We characterised the basal properties of the onset region of NEGIS and discussed involved physical processes. The analysis of basal roughness and basal return echoes shows a distinct change of basal conditions at the position where the ice stream widens. We conclude that a smooth, deformable and lubricated base helps to initiate or at least favour ice flow acceleration at the onset of the NEGIS. The positioning of the shear margins and the pathways of subglacial water flow shows an immediate relationship between the ice stream extent and the subglacial hydrology system. Regionally extending our interpretation, the involved processes could have a significant impact on the ice dynamics and ice stream catchments of Greenland in a warming climate. Large areas of the Greenland ice sheet show indications for a smooth and temperate bed. With the increase of the area, where melt-generated surface water can drain to the bed, towards higher elevations, more regions could, therefore, become a potential point of initiation of faster ice flow, and potentially develop farther inland reaching ice streams. The drilling of the East Greenland Ice Core down to the bed will provide further insights into NEGIS' characteristics and dynamical processes, especially into fabric distribution, thermal structure, sediment properties and geothermal heat flux. As shown by our analyses, useful additional information to constrain the basal conditions can be provided by spatially extensive and closely-spaced geophysical surveys. Considerable insights could be obtained by further seismic soundings further upstream and downstream and borehole drilling to the base. However, these are time-consuming and expensive to acquire over a large area. To fully constrain the basal boundary conditions for ice flow models, a sufficient coverage of the middle and lower sections of NEGIS are needed.

Data availability

All relevant datasets for this research are available from the PANGAEA repository: EGRIP-NOR-2018 bed topography (Franke et al. (2019); https://doi.pangaea.de/10.1594/PANGAEA.907918) and radar-derived basal conditions data (Franke et al., 2020a), which contains spectral basal roughness data (https://doi.pangaea.de/10.1594/PANGAEA.915133), bed return power and scattering derived abruptness waveform data (https://doi.pangaea.de/10.1594/PANGAEA.915135) as well as basal water routing (https://doi.pangaea.de/10.1594/PANGAEA.915134). The BedMachine v3 bed elevation data set is available at the National Snow and Ice Data Center (NSIDC): https://doi.org/10.5067/2CIX82HUV88Y. The MEaSUREs Greenland Ice Sheet Velocity Map from InSAR Data, Version 2 is available from https://doi.org/10.5067/OC7B04ZM9G6Q.

Acknowledgements

We thank the Ken Borek crew and AWI's aeroplane technical staff of the research aircraft Polar 6. Logistical support in the field was provided by the East Greenland Ice-Core Project (EGRIP). EGRIP is directed and organised by the Center of Ice and Climate at the Niels Bohr Institute. It is supported by funding agencies and institutions in Denmark (A. P. Møller Foundation, University of Copenhagen), USA (US National Science Foundation, Office of Polar Programs), Germany (Alfred Wegener Institute, Helmholtz Centre for Polar and Marine Research), Japan (National Institute of Polar Research and Arctic Challenge for Sustainability), Norway (University of Bergen and Bergen Research Foundation), Switzerland (Swiss National Science Foundation), France (French Polar Institute Paul-Emile Victor, Institute for Geosciences and Environmental research) and China (Chinese Academy of Sciences and Beijing Normal University). We acknowledge the use of the CReSIS toolbox from CReSIS generated with support from the University of Kansas, NASA Operation IceBridge grant NNX16AH54G, and NSF grants ACI-1443054, OPP-1739003, and IIS-1838230. The analysis of spectral basal roughness parameters builds on the work by Franz-Fabian Bellot and Eythor Gudlaugsson under the supervision of Angelika Humbert. We acknowledge the discussion with Thomas Kleiner, which helped to develop and improve the manuscript. Furthermore, we thank Giulia Sinnl and Enrico Pochini. They performed a first initial analysis of the spectral basal roughness during the Karthaus Summer School 2019 organised by the Institute for Marine and Atmospheric research Utrecht (IMAU).

Author contributions

Steven Franke designed and wrote the manuscript and conducted the radar data processing and analysis of subglacial spectral roughness and bed return echoes. Olaf Eisen and Daniela Jansen were PI and Co-I of the airborne radar campaign and designed the study. Sebastian Beyer computed the hydraulic potential and basal water pathways. Tobias Binder recorded the radar data together with Daniela Jansen and John Paden. Tobias Binder contributed to the radar data processing and John Paden to the analysis of bed return echoes. Daniela Jansen, Steven Franke, Sebastian Beyer and Olaf Eisen interpreted the data. All co-authors discussed and commented on the manuscript.

Appendix

Uncertainties

Several uncertainties can influence the results and interpretation of the spectral bed roughness parameters. This accounts in particular for small values of ξ in conjunction with η. A major uncertainty arises from missing or ambiguous bed reflections and how continuous the tracking of the basal event is applied. In rough terrains, automatic trackers, e.g. of reflection power, often create zigzag or step patterns whereas manual picking is often characterised by straight lines. A combination of both methods may represent the best possible way to pick the bed geometry efficiently. Still, it will have an impact on both vertical and horizontal roughness values, in particular when ξ is small. The uncertainty decreases if larger vertical amplitudes come into play. Li et al.

(2010) introduced schematic interpretations for geomorphic settings based on the combination of ξ and $\eta_|$, which we will refer to as cases in the following. For example, low ξ and high $\eta_|$ (case 1) can refer to a marine setting with intensive deposition of sediments. Low ξ and low $\eta_|$ (case 2) could imply a continental setting after intensive erosion. For minimal values of ξ, this categorisation is accompanied with a high uncertainty based on the radar data or bed topography product and the method of the ice-bed interface detection. For example, automatic or semiautomatic picking with a maximum power tracker might lead to a high-frequency zigzag pattern leading to case 2 (erosion). Manual picking at locations where a tracker is not useful can smooth the surface and would favour case 1 (deposition). Therefore, we argue that an interpretation of subglacial landscapes with low ξ are difficult to interpret in combination with $\eta_|$, even though the bed reflection is quality checked and picked very accurately. A robust interpretation of small ξ, regardless of high or low $\eta_|$, is that the base is smooth. Without additional data like radar wave scattering properties, seismic information about the basal substrate's lithology, or an indication for the presence of water at the base, further interpretations have low confidence. Another source of uncertainty are off-nadir/side reflections that are difficult to distinguish from nadir reflections. Only coherent and phase-sensitive radar depth sounders with multiple cross-track antenna elements and appropriate 3D processing algorithms can compute the direction angle of the reflected signal (Paden et al., 2010). A better estimate of the effect of cross-track roughness is the scattering-derived waveform abruptness (Oswald and Gogineni, 2008; Jordan et al., 2017; Cooper et al., 2019). However, this method does not consider side reflections from far off-nadir angles.

Several uncertainties result from the mostly unobserved physical bulk properties of the ice column and their lateral variation, mainly across the ice stream. We anticipate an effect of ice crystal anisotropy on the basal return signal due to a different expected preferred orientation in the crystal fabric in the ice stream, outside of the ice stream and in the area of the shear margins. However, overall we consider it as a negligible effect on the BRP (Matsuoka, 2011), given the magnitude of other uncertainties. The most significant uncertainty will arise from the unknown dielectric attenuation of the ice column from impurity loading and temperature, which is difficult to estimate for an ice stream. It is challenging to estimate the effect of englacial attenuation in our survey area because ice temperature has not been sufficiently constrained yet. For an ice stream, we have to consider three different lateral domains, with unknown dielectric attenuation: the fast-flowing central part of streaming ice, the slow-flowing part outside of the ice stream and the shear margins. Finally, in general, a layer of temperate ice of finite thickness might be present above the bed (Humbert et al., 2018). As we cannot constrain its presence further because of missing measurements, we do not consider it in our evaluation. An additional feature, influencing the bed return intensity can be internal layers of altered ice or containing entrainments of basal material which reduce the return energy of the bed. We find areas of large folds south-west of the EGRIP drill site outside of the ice stream. Therefore, we excluded this region because the strong internal deformation and bed entrainments appear to disturb the reflection power of the base significantly.

Further uncertainties are related to data acquisition and processing. Another source of uncertainty for the BRP can arise during SAR processing of the radar data. Focusing of scattered signals effectively shifts energy from multiple unfocused pixels into a single pixel. As a consequence, poor focusing due to position errors or directional scattering may cause the return power to deviate from the ideal case. Furthermore, the steeply dipping reflectors due to englacial layer folding in the vicinity of the shear margins will most likely reduce the reflected energy from the ice-basal interface

underneath this zone. The energy loss probably occurs due to destructive interference in trace stacking, energy dispersion through SAR processing and off-nadir ray path losses (see Holschuh et al. (2014) for details).

References

Lu An, Eric Rignot, Nolwenn Chauche, David M. Holland, Denise Holland, Martin Jakobsson, Emily Kane, Michael Wood, Ingo Klaucke, Mathieu Morlighem, Isabella Velicogna, Wilhelm Weinrebe, and Josh K. Willis. Bathymetry of Southeast Greenland From Oceans Melting Greenland (OMG) Data. *Geophysical Research Letters*, 46(20):11197–11205, oct 2019. doi: 10.1029/2019gl083953. URL https://doi.org/10.1029%2F2019gl083953.

Jan Erik Arndt, Robert D. Larter, Claus-Dieter Hillenbrand, Simon H. Sørli, Matthias Forwick, James A. Smith, and Lukas Wacker. Past ice sheet-seabed interactions in the northeastern Weddell Sea Embayment Antarctica. dec 2019. doi: 10.5194/tc-2019-271. URL https://doi.org/10.5194%2Ftc-2019-271.

Emily Arnold, Carl Leuschen, Fernando Rodriguez-Morales, Jilu Li, John Paden, Richard Hale, and Shawn Keshmiri. CReSIS airborne radars and platforms for ice and snow sounding. *Annals of Glaciology*, pages 1–10, nov 2019. doi: 10.1017/aog.2019.37. URL https://doi.org/10.1017%2Faog.2019.37.

Andy Aschwanden, Mark A. Fahnestock, and Martin Truffer. Complex Greenland outlet glacier flow captured. *Nature Communications*, 7(1), feb 2016. doi: 10.1038/ncomms10524. URL https://doi.org/10.1038%2Fncomms10524.

Robert G. Bingham and Martin J. Siegert. Radar-derived bed roughness characterization of Institute and Möller ice streams West Antarctica, and comparison with Siple Coast ice streams. *Geophysical Research Letters*, 34(21), nov 2007. doi: 10.1029/2007gl031483. URL https://doi.org/10.1029%2F2007gl031483.

Robert G. Bingham and Martin J. Siegert. Quantifying subglacial bed roughness in Antarctica: implications for ice-sheet dynamics and history. *Quaternary Science Reviews*, 28(3-4):223–236, feb 2009. doi: 10.1016/j.quascirev.2008.10.014. URL https://doi.org/10.1016%2Fj.quascirev.2008.10.014.

Robert G. Bingham, David G. Vaughan, Edward C. King, Damon Davies, Stephen L. Cornford, Andrew M. Smith, Robert J. Arthern, Alex M. Brisbourne, Jan De Rydt, Alastair G. C. Graham, Matteo Spagnolo, Oliver J. Marsh, and David E. Shean. Diverse landscapes beneath Pine Island Glacier influence ice flow. *Nature Communications*, 8(1), nov 2017. doi: 10.1038/s41467-017-01597-y. URL https://doi.org/10.1038%2Fs41467-017-01597-y.

P. D. Bons, T. Kleiner, M.-G. Llorens, D. J. Prior, T. Sachau, I. Weikusat, and D. Jansen. Greenland Ice Sheet: Higher Nonlinearity of Ice Flow Significantly Reduces Estimated Basal Motion. *Geophysical Research Letters*, 45(13):6542–6548, jul 2018. doi: 10.1029/2018gl078356. URL https://doi.org/10.1029%2F2018gl078356.

M. Bougamont, P. Christoffersen, A. L Hubbard, A. A. Fitzpatrick, S. H. Doyle, and S. P. Carter. Sensitive response of the Greenland Ice Sheet to surface melt drainage over a soft bed. *Nature*

Communications, 5(1), sep 2014. doi: 10.1038/ncomms6052. URL https://doi.org/10.1038%2Fncomms6052.

A. M. Brisbourne, A. M. Smith, E. C. King, K. W. Nicholls, P. R. Holland, and K. Makinson. Seabed topography beneath Larsen C Ice Shelf from seismic soundings. *The Cryosphere*, 8(1): 1–13, jan 2014. doi: 10.5194/tc-8-1-2014. URL https://doi.org/10.5194%2Ftc-8-1-2014.

A. M. Brisbourne, A. M. Smith, D. G. Vaughan, E. C. King, D. Davies, R. G. Bingham, E. C. Smith, I. J. Nias, and S. H. R. Rosier. Bed conditions of Pine Island Glacier West Antarctica. *Journal of Geophysical Research: Earth Surface*, 122(1):419–433, jan 2017. doi: 10.1002/2016jf004033. URL https://doi.org/10.1002%2F2016jf004033.

Reinhard Calov, Sebastian Beyer, Ralf Greve, Johanna Beckmann, Matteo Willeit, Thomas Kleiner, Martin Rückamp, Angelika Humbert, and Andrey Ganopolski. Simulation of the future sea level contribution of Greenland with a new glacial system model. *The Cryosphere*, 12(10):3097–3121, oct 2018. doi: 10.5194/tc-12-3097-2018. URL https://doi.org/10.5194%2Ftc-12-3097-2018.

Knut Christianson, Leo E. Peters, Richard B. Alley, Sridhar Anandakrishnan, Robert W. Jacobel, Kiya L. Riverman, Atsuhiro Muto, and Benjamin A. Keisling. Dilatant till facilitates ice-stream flow in northeast Greenland. *Earth and Planetary Science Letters*, 401:57–69, sep 2014. doi: 10.1016/j.epsl.2014.05.060. URL https://doi.org/10.1016%2Fj.epsl.2014.05.060.

Chris D. Clark and Robert T. Meehan. Subglacial bedform geomorphology of the Irish Ice Sheet reveals major configuration changes during growth and decay. *Journal of Quaternary Science*, 16 (5):483–496, 2001. doi: 10.1002/jqs.627. URL https://doi.org/10.1002%2Fjqs.627.

Garry K.C. Clarke. SUBGLACIAL PROCESSES. *Annual Review of Earth and Planetary Sciences*, 33(1):247–276, may 2005. doi: 10.1146/annurev.earth.33.092203.122621. URL https://doi.org/10.1146%2Fannurev.earth.33.092203.122621.

James R. Cochran and Robin E. Bell. Inversion of IceBridge gravity data for continental shelf bathymetry beneath the Larsen Ice Shelf Antarctica. *Journal of Glaciology*, 58(209):540–552, 2012. doi: 10.3189/2012jog11j033. URL https://doi.org/10.3189%2F2012jog11j033.

Michael A. Cooper, Thomas M. Jordan, Dustin M. Schroeder, Martin J. Siegert, Christopher N. Williams, and Jonathan L. Bamber. Subglacial roughness of the Greenland Ice Sheet: relationship with contemporary ice velocity and geology. *The Cryosphere*, 13(11):3093–3115, nov 2019. doi: 10.5194/tc-13-3093-2019. URL https://doi.org/10.5194%2Ftc-13-3093-2019.

Hugh Corr, John C. Moore, and Keith W. Nicholls. Radar absorption due to impurities in Antarctic ice. *Geophysical Research Letters*, 20(11):1071–1074, jun 1993. doi: 10.1029/93gl01395. URL https://doi.org/10.1029%2F93gl01395.

T. Cowton, P. Nienow, I. Bartholomew, A. Sole, and D. Mair. Rapid erosion beneath the Greenland ice sheet. *Geology*, 40(4):343–346, apr 2012. doi: 10.1130/g32687.1. URL https://doi.org/10.1130%2Fg32687.1.

Anja Diez, Kenichi Matsuoka, Fausto Ferraccioli, Tom A. Jordan, Hugh F. Corr, Jack Kohler, Arne V. Olesen, and René Forsberg. Basal Settings Control Fast Ice Flow in the Recovery/Slessor/Bailey Region East Antarctica. *Geophysical Research Letters*, 45(6):2706–2715, mar 2018. doi: 10.1002/2017gl076601. URL https://doi.org/10.1002%2F2017gl076601.

C.F. Dow, A. Hubbard, A.D. Booth, S.H. Doyle, A. Gusmeroli, and B. Kulessa. Seismic evidence of mechanically weak sediments underlying Russell Glacier West Greenland. *Annals of Glaciology*, 54(64):135–141, 2013. doi: 10.3189/2013aog64a032. URL https://doi.org/10.3189%2F2013aog64a032.

Julian A. Dowdeswell, Colm Ó Cofaigh, and Carol J. Pudsey. Thickness and extent of the subglacial till layer beneath an Antarctic paleo–ice stream. *Geology*, 32(1):13, 2004. doi: 10.1130/g19864.1. URL https://doi.org/10.1130%2Fg19864.1.

G. Durand, O. Gagliardini, L. Favier, T. Zwinger, and E. le Meur. Impact of bedrock description on modeling ice sheet dynamics. *Geophysical Research Letters*, 38(20):n/a–n/a, oct 2011. doi: 10.1029/2011gl048892. URL https://doi.org/10.1029%2F2011gl048892.

Olaf Eisen, Anna Winter, Daniel Steinhage, Thomas Kleiner, and Angelika Humbert. Basal roughness of the East Antarctic Ice Sheet and indications for the basal thermal state. *Annals of Glaciology (in press)*, pages 1–14, 2020.

H. Eisermann, G. Eagles, A. Ruppel, E. C. Smith, and W. Jokat. Bathymetry beneath ice shelves of western dronning maud land, east antarctica, and implications on ice shelf stability. *Geophysical Research Letters*, n/a(n/a):e2019GL086724, 2020. doi: 10.1029/2019GL086724. URL https://agupubs.onlinelibrary.wiley.com/doi/abs/10.1029/2019GL086724. e2019GL086724 2019GL086724.

M. Fahnestock. High Geothermal Heat Flow Basal Melt, and the Origin of Rapid Ice Flow in Central Greenland. *Science*, 294(5550):2338–2342, dec 2001. doi: 10.1126/science.1065370. URL https://doi.org/10.1126%2Fscience.1065370.

M. Fahnestock, R. Bindschadler, R. Kwok, and K. Jezek. Greenland Ice Sheet Surface Properties and Ice Dynamics from ERS-1 SAR Imagery. *Science*, 262(5139):1530–1534, dec 1993. doi: 10.1126/science.262.5139.1530. URL https://doi.org/10.1126%2Fscience.262.5139.1530.

Francesca A.M. Falcini, David M. Rippin, Maarten Krabbendam, and Katherine A. Selby. Quantifying bed roughness beneath contemporary and palaeo-ice streams. *Journal of Glaciology*, 64(247):822–834, sep 2018. doi: 10.1017/jog.2018.71. URL https://doi.org/10.1017%2Fjog.2018.71.

Steven Franke, Daniela Jansen, Tobias Binder, Nils Dörr, John Paden, Veit Helm, Daniel Steinhage, and Olaf Eisen. Bedrock topography and ice thickness in the onset region of the Northeast Greenland Ice Stream recorded with the airborne AWI Ultra-Wideband radar (UWB) in 2018, 2019. URL https://doi.pangaea.de/10.1594/PANGAEA.907918.

Steven Franke, Daniela Jansen, Sebastian Beyer, John Paden, and Olaf Eisen. Basal conditions of the onset zone of the Northeast Greenland Ice Stream derived from airborne ultra-wideband radar data. *PANGAEA*, 2020a. doi: 10.1594/PANGAEA.915136.

Steven Franke, Daniela Jansen, Tobias Binder, Nils Dörr, Veit Helm, John Paden, Daniel Steinhage, and Olaf Eisen. Bed topography and subglacial landforms in the onset region of the Northeast Greenland Ice Stream. *Annals of Glaciology*, pages 1–11, mar 2020b. doi: 10.1017/aog.2020.12. URL https://doi.org/10.1017%2Faog.2020.12.

P. Fretwell, H. D. Pritchard, D. G. Vaughan, J. L. Bamber, N. E. Barrand, R. Bell, C. Bianchi, R. G. Bingham, D. D. Blankenship, G. Casassa, G. Catania, D. Callens, H. Conway, A. J. Cook,

H. F. J. Corr, D. Damaske, V. Damm, F. Ferraccioli, R. Forsberg, S. Fujita, Y. Gim, P. Gogineni, J. A. Griggs, R. C. A. Hindmarsh, P. Holmlund, J. W. Holt, R. W. Jacobel, A. Jenkins, W. Jokat, T. Jordan, E. C. King, J. Kohler, W. Krabill, M. Riger-Kusk, K. A. Langley, G. Leitchenkov, C. Leuschen, B. P. Luyendyk, K. Matsuoka, J. Mouginot, F. O. Nitsche, Y. Nogi, O. A. Nost, S. V. Popov, E. Rignot, D. M. Rippin, A. Rivera, J. Roberts, N. Ross, M. J. Siegert, A. M. Smith, D. Steinhage, M. Studinger, B. Sun, B. K. Tinto, B. C. Welch, D. Wilson, D. A. Young, C. Xiangbin, and A. Zirizzotti. Bedmap2: improved ice bed surface and thickness datasets for Antarctica. *The Cryosphere*, 7(1):375–393, feb 2013. doi: 10.5194/tc-7-375-2013. URL https://doi.org/10.5194%2Ftc-7-375-2013.

Christoph Förste, Roland Schmidt, Richard Stubenvoll, Frank Flechtner, Ulrich Meyer, Rolf König, Hans Neumayer, Richard Biancale, Jean-Michel Lemoine, Sean Bruinsma, Sylvain Loyer, Franz Barthelmes, and Saskia Esselborn. The GeoForschungsZentrum Potsdam/Groupe de Recherche de Gèodésie Spatiale satellite-only and combined gravity field models: EIGEN-GL04S1 and EIGEN-GL04C. *Journal of Geodesy*, 82(6):331–346, oct 2007. doi: 10.1007/s00190-007-0183-8. URL https://doi.org/10.1007%2Fs00190-007-0183-8.

E. Gudlaugsson, A. Humbert, M. Winsborrow, and K. Andreassen. Subglacial roughness of the former Barents Sea ice sheet. *Journal of Geophysical Research: Earth Surface*, 118(4):2546–2556, dec 2013. doi: 10.1002/2013jf002714. URL https://doi.org/10.1002%2F2013jf002714.

R. Hale, H. Miller, S. Gogineni, J. B. Yan, F. Rodriguez-Morales, C. Leuschen, J. Paden, J. Li, T. Binder, D. Steinhage, M. Gehrmann, and D. Braaten. Multi-channel ultra-wideband radar sounder and imager. In *2016 IEEE International Geoscience and Remote Sensing Symposium (IGARSS)*. IEEE, jul 2016. doi: 10.1109/igarss.2016.7729545. URL https://doi.org/10.1109%2Figarss.2016.7729545.

C. Hofstede, P. Christoffersen, B. Hubbard, S. H. Doyle, T. J. Young, A. Diez, O. Eisen, and A. Hubbard. Physical Conditions of Fast Glacier Flow: 2. Variable Extent of Anisotropic Ice and Soft Basal Sediment From Seismic Reflection Data Acquired on Store Glacier West Greenland. *Journal of Geophysical Research: Earth Surface*, 123(2):349–362, feb 2018. doi: 10.1002/2017jf004297. URL https://doi.org/10.1002%2F2017jf004297.

Nicholas Holschuh, Knut Christianson, and Sridhar Anandakrishnan. Power loss in dipping internal reflectors imaged using ice-penetrating radar. *Annals of Glaciology*, 55(67):49–56, 2014. doi: 10.3189/2014aog67a005. URL https://doi.org/10.3189%2F2014aog67a005.

Bryn Hubbard, Martin J. Siegert, and Danny McCarroll. Spectral roughness of glaciated bedrock geomorphic surfaces: Implications for glacier sliding. *Journal of Geophysical Research: Solid Earth*, 105(B9):21295–21303, sep 2000. doi: 10.1029/2000jb900162. URL https://doi.org/10.1029%2F2000jb900162.

Terence Hughes, Aitbala Sargent, and James Fastook. Ice-bed coupling beneath and beyond ice streams: Byrd Glacier Antarctica. *Journal of Geophysical Research*, 116(F3), jul 2011. doi: 10.1029/2010jf001896. URL https://doi.org/10.1029%2F2010jf001896.

Angelika Humbert, Daniel Steinhage, Veit Helm, Sebastian Beyer, and Thomas Kleiner. Missing Evidence of Widespread Subglacial Lakes at Recovery Glacier Antarctica. *Journal of Geophysical*

Research: Earth Surface, 123(11):2802–2826, nov 2018. doi: 10.1029/2017jf004591. URL https://doi.org/10.1029%2F2017jf004591.

R. W. Jacobel, K. E. Lapo, J. R. Stamp, B. W. Youngblood, B. C. Welch, and J. L. Bamber. A comparison of basal reflectivity and ice velocity in East Antarctica. *The Cryosphere*, 4(4):447–452, oct 2010. doi: 10.5194/tc-4-447-2010. URL https://doi.org/10.5194%2Ftc-4-447-2010.

T. M. Jordan, J. L. Bamber, C. N. Williams, J. D. Paden, M. J. Siegert, P. Huybrechts, O. Gagliardini, and F. Gillet-Chaulet. An ice-sheet-wide framework for englacial attenuation from ice-penetrating radar data. *The Cryosphere*, 10(4):1547–1570, jul 2016. doi: 10.5194/tc-10-1547-2016. URL https://doi.org/10.5194%2Ftc-10-1547-2016.

Thomas M. Jordan, Michael A. Cooper, Dustin M. Schroeder, Christopher N. Williams, John D. Paden, Martin J. Siegert, and Jonathan L. Bamber. Self-affine subglacial roughness: consequences for radar scattering and basal water discrimination in northern Greenland. *The Cryosphere*, 11 (3):1247–1264, may 2017. doi: 10.5194/tc-11-1247-2017. URL https://doi.org/10.5194%2Ftc-11-1247-2017.

Thomas M. Jordan, Christopher N. Williams, Dustin M. Schroeder, Yasmina M. Martos, Michael A. Cooper, Martin J. Siegert, John D. Paden, Philippe Huybrechts, and Jonathan L. Bamber. A constraint upon the basal water distribution and thermal state of the Greenland Ice Sheet from radar bed echoes. *The Cryosphere*, 12(9):2831–2854, sep 2018. doi: 10.5194/tc-12-2831-2018. URL https://doi.org/10.5194%2Ftc-12-2831-2018.

Ian Joughin, Mark Fahnestock, Doug MacAyeal, Jonathan L. Bamber, and Prasad Gogineni. Observation and analysis of ice flow in the largest Greenland ice stream. *Journal of Geophysical Research: Atmospheres*, 106(D24):34021–34034, dec 2001. doi: 10.1029/2001jd900087. URL https://doi.org/10.1029%2F2001jd900087.

Ian Joughin, Ben E. Smith, and Ian M. Howat. A complete map of Greenland ice velocity derived from satellite data collected over 20 years. *Journal of Glaciology*, 64(243):1–11, nov 2017. doi: 10.1017/jog.2017.73. URL https://doi.org/10.1017%2Fjog.2017.73.

N. B. Karlsson and D. Dahl-Jensen. Response of the large-scale subglacial drainage system of Northeast Greenland to surface elevation changes. *The Cryosphere*, 9(4):1465–1479, aug 2015. doi: 10.5194/tc-9-1465-2015. URL https://doi.org/10.5194%2Ftc-9-1465-2015.

Benjamin A. Keisling, Knut Christianson, Richard B. Alley, Leo E. Peters, John E.M. Christian, Sridhar Anandakrishnan, Kiya L. Riverman, Atsuhiro Muto, and Robert W. Jacobel. Basal conditions and ice dynamics inferred from radar-derived internal stratigraphy of the northeast Greenland ice stream. *Annals of Glaciology*, 55(67):127–137, 2014. doi: 10.3189/2014aog67a090. URL https://doi.org/10.3189%2F2014aog67a090.

E. C. King, R. C. A. Hindmarsh, and C. R. Stokes. Formation of mega-scale glacial lineations observed beneath a West Antarctic ice stream. *Nature Geoscience*, 2(8):585–588, jul 2009. doi: 10.1038/ngeo581. URL https://doi.org/10.1038%2Fngeo581.

Maarten Krabbendam, Nick Eyles, Niko Putkinen, Tom Bradwell, and Lina Arbelaez-Moreno. Streamlined hard beds formed by palaeo-ice streams: A review. *Sedimentary Geology*, 338:24–

50, jun 2016. doi: 10.1016/j.sedgeo.2015.12.007. URL https://doi.org/10.1016%2Fj.sedgeo.2015.12.007.

Bernd Kulessa, Alun L. Hubbard, Adam D. Booth, Marion Bougamont, Christine F. Dow, Samuel H. Doyle, Poul Christoffersen, Katrin Lindbäck, Rickard Pettersson, Andrew A. W. Fitzpatrick, and Glenn A. Jones. Seismic evidence for complex sedimentary control of Greenland Ice Sheet flow. *Science Advances*, 3(8):e1603071, aug 2017. doi: 10.1126/sciadv.1603071. URL https://doi.org/10.1126%2Fsciadv.1603071.

E. Larour, J. Utke, B. Csatho, A. Schenk, H. Seroussi, M. Morlighem, E. Rignot, N. Schlegel, and A. Khazendar. Inferred basal friction and surface mass balance of the Northeast Greenland Ice Stream using data assimilation of ICESat (Ice Cloud and land Elevation Satellite) surface altimetry and ISSM (Ice Sheet System Model). *The Cryosphere*, 8(6):2335–2351, dec 2014. doi: 10.5194/tc-8-2335-2014. URL https://doi.org/10.5194%2Ftc-8-2335-2014.

R. L. Layberry and J. L. Bamber. A new ice thickness and bed data set for the Greenland ice sheet: 2. Relationship between dynamics and basal topography. *Journal of Geophysical Research: Atmospheres*, 106(D24):33781–33788, dec 2001. doi: 10.1029/2001jd900053. URL https://doi.org/10.1029%2F2001jd900053.

Anne M Le Brocq, Antony J Payne, and Martin J Siegert. West Antarctic balance calculations: Impact of flux-routing algorithm smoothing algorithm and topography. *Computers & Geosciences*, 32(10):1780–1795, dec 2006. doi: 10.1016/j.cageo.2006.05.003. URL https://doi.org/10.1016%2Fj.cageo.2006.05.003.

Anne M Le Brocq, A.J. Payne, M.J. Siegert, and R.B. Alley. A subglacial water-flow model for West Antarctica. *Journal of Glaciology*, 55(193):879–888, 2009. doi: 10.3189/002214309790152564. URL https://doi.org/10.3189%2F002214309790152564.

Xin Li, Bo Sun, Martin J. Siegert, Robert G. Bingham, Xueyuan Tang, Dong Zhang, Xiangbin Cui, and Xiangpei Zhang. Characterization of subglacial landscapes by a two-parameter roughness index. *Journal of Glaciology*, 56(199):831–836, 2010. doi: 10.3189/002214310794457326. URL https://doi.org/10.3189%2F002214310794457326.

K. Lindbäck and R. Pettersson. Spectral roughness and glacial erosion of a land-terminating section of the Greenland Ice Sheet. *Geomorphology*, 238:149–159, jun 2015. doi: 10.1016/j.geomorph.2015.02.027. URL https://doi.org/10.1016%2Fj.geomorph.2015.02.027.

S. J. Livingstone, C. D. Clark, J. Woodward, and J. Kingslake. Potential subglacial lake locations and meltwater drainage pathways beneath the Antarctic and Greenland ice sheets. *The Cryosphere*, 7 (6):1721–1740, nov 2013. doi: 10.5194/tc-7-1721-2013. URL https://doi.org/10.5194%2Ftc-7-1721-2013.

Joseph A. MacGregor, Ginny A. Catania, Howard Conway, Dustin M. Schroeder, Ian Joughin, Duncan A. Young, Scott D. Kempf, and Donald D. Blankenship. Weak bed control of the eastern shear margin of Thwaites Glacier West Antarctica. *Journal of Glaciology*, 59(217):900–912, 2013. doi: 10.3189/2013jog13j050. URL https://doi.org/10.3189%2F2013jog13j050.

Joseph A. MacGregor, Mark A. Fahnestock, Ginny A. Catania, Andy Aschwanden, Gary D. Clow, William T. Colgan, S. Prasad Gogineni, Mathieu Morlighem, Sophie M. J. Nowicki, John D.

960 Paden, Stephen F. Price, and Hélène Seroussi. A synthesis of the basal thermal state of the
961 Greenland Ice Sheet. *Journal of Geophysical Research: Earth Surface*, 121(7):1328–1350, jul 2016.
962 doi: 10.1002/2015jf003803. URL https://doi.org/10.1002%2F2015jf003803.

963 Kenichi Matsuoka. Pitfalls in radar diagnosis of ice-sheet bed conditions: Lessons from englacial
964 attenuation models. *Geophysical Research Letters*, 38(5):n/a–n/a, mar 2011. doi: 10.1029/
965 2010gl046205. URL https://doi.org/10.1029%2F2010gl046205.

966 Kenichi Matsuoka, Frank Pattyn, Denis Callens, and Howard Conway. Radar characterization of the
967 basal interface across the grounding zone of an ice-rise promontory in East Antarctica. *Annals of*
968 *Glaciology*, 53(60):29–34, 2012. doi: 10.3189/2012aog60a106. URL https://doi.org/10.3189%
969 2F2012aog60a106.

970 Colin R. Meyer, Alissar Yehya, Brent Minchew, and James R. Rice. A Model for the Downstream
971 Evolution of Temperate Ice and Subglacial Hydrology Along Ice Stream Shear Margins. *Journal*
972 *of Geophysical Research: Earth Surface*, 123(8):1682–1698, aug 2018. doi: 10.1029/2018jf004669.
973 URL https://doi.org/10.1029%2F2018jf004669.

974 M. Morlighem, C. N. Williams, E. Rignot, L. An, J. E. Arndt, J. L. Bamber, G. Catania, N. Chauché,
975 J. A. Dowdeswell, B. Dorschel, I. Fenty, K. Hogan, I. Howat, A. Hubbard, M. Jakobsson,
976 T. M. Jordan, K. K. Kjeldsen, R. Millan, L. Mayer, J. Mouginot, B. P. Y. Noël, C. O'Cofaigh,
977 S. Palmer, S. Rysgaard, H. Seroussi, M. J. Siegert, P. Slabon, F. Straneo, M. R. van den Broeke,
978 W. Weinrebe, M. Wood, and K. B. Zinglersen. BedMachine v3: Complete Bed Topography
979 and Ocean Bathymetry Mapping of Greenland From Multibeam Echo Sounding Combined
980 With Mass Conservation. *Geophysical Research Letters*, 44(21):11,051–11,061, nov 2017. doi:
981 10.1002/2017gl074954. URL https://doi.org/10.1002%2F2017gl074954.

982 Mathieu Morlighem, Eric Rignot, Tobias Binder, Donald Blankenship, Reinhard Drews, Graeme
983 Eagles, Olaf Eisen, Fausto Ferraccioli, René Forsberg, Peter Fretwell, Vikram Goel, Jamin S.
984 Greenbaum, Hilmar Gudmundsson, Jingxue Guo, Veit Helm, Coen Hofstede, Ian Howat, Angelika
985 Humbert, Wilfried Jokat, Nanna B. Karlsson, Won Sang Lee, Kenichi Matsuoka, Romain Millan,
986 Jeremie Mouginot, John Paden, Frank Pattyn, Jason Roberts, Sebastian Rosier, Antonia Ruppel,
987 Helene Seroussi, Emma C. Smith, Daniel Steinhage, Bo Sun, Michiel R. van den Broeke, Tas D. van
988 Ommen, Melchior van Wessem, and Duncan A. Young. Deep glacial troughs and stabilizing ridges
989 unveiled beneath the margins of the Antarctic ice sheet. *Nature Geoscience*, 13(2):132–137, dec
990 2019. doi: 10.1038/s41561-019-0510-8. URL https://doi.org/10.1038%2Fs41561-019-0510-8.

991 Atsuhiro Muto, Sidhar Anandakrishnan, and Richard B. Alley. Subglacial bathymetry and sediment
992 layer distribution beneath the Pine Island Glacier ice shelf West Antarctica, modeled using
993 aerogravity and autonomous underwater vehicle data. *Annals of Glaciology*, 54(64):27–32, 2013.
994 doi: 10.3189/2013aog64a110. URL https://doi.org/10.3189%2F2013aog64a110.

995 G.K.A. Oswald and S.P. Gogineni. Recovery of subglacial water extent from Greenland radar survey
996 data. *Journal of Glaciology*, 54(184):94–106, 2008. doi: 10.3189/002214308784409107. URL
997 https://doi.org/10.3189%2F002214308784409107.

998 Gordon K. A. Oswald and S. P. Gogineni. Mapping Basal Melt Under the Northern Greenland
999 Ice Sheet. *IEEE Transactions on Geoscience and Remote Sensing*, 50(2):585–592, feb 2012. doi:
1000 10.1109/tgrs.2011.2162072. URL https://doi.org/10.1109%2Ftgrs.2011.2162072.

John Paden, Torry Akins, David Dunson, Chris Allen, and Prasad Gogineni. Ice-sheet bed 3-D tomography. *Journal of Glaciology*, 56(195):3–11, 2010. doi: 10.3189/002214310791190811. URL https://doi.org/10.3189%2F002214310791190811.

Thibaut Perol and James R. Rice. Shear heating and weakening of the margins of West Antarctic ice streams. *Geophysical Research Letters*, 42(9):3406–3413, may 2015. doi: 10.1002/2015gl063638. URL https://doi.org/10.1002%2F2015gl063638.

Thibaut Perol, James R. Rice, John D. Platt, and Jenny Suckale. Subglacial hydrology and ice stream margin locations. *Journal of Geophysical Research: Earth Surface*, 120(7):1352–1368, jul 2015. doi: 10.1002/2015jf003542. URL https://doi.org/10.1002%2F2015jf003542.

R.K. Raney. The delay/Doppler radar altimeter. *IEEE Transactions on Geoscience and Remote Sensing*, 36(5):1578–1588, 1998. doi: 10.1109/36.718861. URL https://doi.org/10.1109%2F36.718861.

David M. Rippin. Bed roughness beneath the Greenland ice sheet. *Journal of Glaciology*, 59(216): 724–732, 2013. doi: 10.3189/2013jog12j212. URL https://doi.org/10.3189%2F2013jog12j212.

D.M. Rippin, J.L. Bamber, M.J. Siegert, D.G. Vaughan, and H.F.J. Corr. Basal conditions beneath enhanced-flow tributaries of Slessor Glacier East Antarctica. *Journal of Glaciology*, 52(179):481–490, 2006. doi: 10.3189/172756506781828467. URL https://doi.org/10.3189%2F172756506781828467.

D.M. Rippin, D.G. Vaughan, and H.F.J. Corr. The basal roughness of Pine Island Glacier West Antarctica. *Journal of Glaciology*, 57(201):67–76, 2011. doi: 10.3189/002214311795306574. URL https://doi.org/10.3189%2F002214311795306574.

D.M. Rippin, R.G. Bingham, T.A. Jordan, A.P. Wright, N. Ross, H.F.J. Corr, F. Ferraccioli, A.M. Le Brocq, K.C. Rose, and M.J. Siegert. Basal roughness of the Institute and Möller Ice Streams West Antarctica: Process determination and landscape interpretation. *Geomorphology*, 214:139–147, jun 2014. doi: 10.1016/j.geomorph.2014.01.021. URL https://doi.org/10.1016%2Fj.geomorph.2014.01.021.

Kiya L. Riverman, Sridhar Anandakrishnan, Richard B. Alley, Nicholas Holschuh, Christine F. Dow, Atsuhiro Muto, Byron R. Parizek, Knut Christianson, and Leo E. Peters. Wet subglacial bedforms of the NE Greenland Ice Stream shear margins. *Annals of Glaciology*, 60(80):91–99, dec 2019. doi: 10.1017/aog.2019.43. URL https://doi.org/10.1017%2Faog.2019.43.

S. H. R. Rosier, C. Hofstede, A. M. Brisbourne, T. Hattermann, K. W. Nicholls, P. E. D. Davis, P. G. D. Anker, C.-D. Hillenbrand, A. M. Smith, and H. F. J. Corr. A New Bathymetry for the Southeastern Filchner-Ronne Ice Shelf: Implications for Modern Oceanographic Processes and Glacial History. *Journal of Geophysical Research: Oceans*, 123(7):4610–4623, jul 2018. doi: 10.1029/2018jc013982. URL https://doi.org/10.1029%2F2018jc013982.

C. Ryser, M. P. Lüthi, L. C. Andrews, G. A. Catania, M. Funk, R. Hawley, M. Hoffman, and T. A. Neumann. Caterpillar-like ice motion in the ablation zone of the Greenland ice sheet. *Journal of Geophysical Research: Earth Surface*, 119(10):2258–2271, oct 2014. doi: 10.1002/2013jf003067. URL https://doi.org/10.1002%2F2013jf003067.

1040 Dustin M. Schroeder, Julian A. Dowdeswell, Martin J. Siegert, Robert G. Bingham, Winnie Chu,
1041 Emma J. MacKie, Matthew R. Siegfried, Katherine I. Vega, John R. Emmons, and Keith
1042 Winstein. Multidecadal observations of the Antarctic ice sheet from restored analog radar
1043 records. *Proceedings of the National Academy of Sciences*, 116(38):18867–18873, sep 2019. doi:
1044 10.1073/pnas.1821646116. URL https://doi.org/10.1073%2Fpnas.1821646116.

1045 Dustin M. Schroeder, Robert G. Bingham, Donald D. Blankenship, Knut Christianson, Olaf Eisen,
1046 Gwenn E. Flowers, Nanna B. Karlsson, Michelle R. Koutnik, John D. Paden, and Martin J.
1047 Siegert. Five decades of radioglaciology. *Annals of Glaciology*, pages 1–13, mar 2020. doi:
1048 10.1017/aog.2020.11. URL https://doi.org/10.1017%2Faog.2020.11.

1049 Michael K. Shepard, Bruce A. Campbell, Mark H. Bulmer, Tom G. Farr, Lisa R. Gaddis, and Jeffrey J.
1050 Plaut. The roughness of natural terrain: A planetary and remote sensing perspective. *Journal*
1051 *of Geophysical Research: Planets*, 106(E12):32777–32795, dec 2001. doi: 10.1029/2000je001429.
1052 URL https://doi.org/10.1029%2F2000je001429.

1053 R. L. Shreve. Movement of Water in Glaciers. *Journal of Glaciology*, 11(62):205–214, 1972. doi:
1054 10.3189/s002214300002219x. URL https://doi.org/10.3189%2Fs002214300002219x.

1055 Martin J. Siegert, Justin Taylor, and Antony J. Payne. Spectral roughness of subglacial topography
1056 and implications for former ice-sheet dynamics in East Antarctica. *Global and Planetary Change*,
1057 45(1-3):249–263, feb 2005. doi: 10.1016/j.gloplacha.2004.09.008. URL https://doi.org/10.
1058 1016%2Fj.gloplacha.2004.09.008.

1059 Martin J. Siegert, Neil Ross, Jilu Li, Dustin M. Schroeder, David Rippin, David Ashmore, Robert
1060 Bingham, and Prasad Gogineni. Subglacial controls on the flow of Institute Ice Stream West
1061 Antarctica. *Annals of Glaciology*, 57(73):19–24, may 2016. doi: 10.1017/aog.2016.17. URL
1062 https://doi.org/10.1017%2Faog.2016.17.

1063 Andrew M. Smith, Tom A. Jordan, Fausto Ferraccioli, and Robert G. Bingham. Influence of
1064 subglacial conditions on ice stream dynamics: Seismic and potential field data from Pine Island
1065 Glacier West Antarctica. *Journal of Geophysical Research: Solid Earth*, 118(4):1471–1482, apr
1066 2013. doi: 10.1029/2012jb009582. URL https://doi.org/10.1029%2F2012jb009582.

1067 Emma C. Smith, Tore Hattermann, Gerhard Kuhn, Christoph Gaedicke, Sophie Berger, Reinhard
1068 Drews, Todd A. Ehlers, Dieter Franke, Rapahel Gromig, Coen Hofstede, Astrid Lambrecht,
1069 Andreas Läufer, Christoph Mayer, Ralf Tiedemann, Frank Wilhelms, and Olaf Eisen. Detailed
1070 seismic bathymetry beneath Ekstroem Ice Shelf Antarctica: Implications for glacial history
1071 and ice-ocean interaction. *Geophysical Research Letters*, page e2019GL086187, may 2020. doi:
1072 10.1029/2019GL086187. URL https://doi.org/10.1029/2019GL086187.

1073 S. Smith-Johnsen, N.-J. Schlegel, B. Fleurian, and K. H. Nisancioglu. Sensitivity of the Northeast
1074 Greenland Ice Stream to Geothermal Heat. *Journal of Geophysical Research: Earth Surface*, 125
1075 (1), jan 2020. doi: 10.1029/2019jf005252. URL https://doi.org/10.1029%2F2019jf005252.

1076 Silje Smith-Johnsen, Basile de Fleurian, Nicole Schlegel, Helene Seroussi, and Kerim Nisanciolgu.
1077 Exceptionally High Geothermal Heat Flux Needed to Sustain the Northeast Greenland Ice Stream.
1078 sep 2019. doi: 10.5194/tc-2019-212. URL https://doi.org/10.5194%2Ftc-2019-212.

1079 L. A. Stearns and C. J. van der Veen. Friction at the bed does not control fast glacier flow. *Science*,

361(6399):273–277, jun 2018. doi: 10.1126/science.aat2217. URL https://doi.org/10.1126%2Fscience.aat2217.

C.R. Stokes, M. Spagnolo, C.D. Clark, C. Ó Cofaigh, O.B. Lian, and R.B. Dunstone. Formation of mega-scale glacial lineations on the Dubawnt Lake Ice Stream bed: 1. size shape and spacing from a large remote sensing dataset. *Quaternary Science Reviews*, 77:190–209, oct 2013. doi: 10.1016/j.quascirev.2013.06.003. URL https://doi.org/10.1016%2Fj.quascirev.2013.06.003.

Justin Taylor, Martin J. Siegert, Antony J. Payne, and Bryn Hubbard. Regional-scale bed roughness beneath ice masses: measurement and analysis. *Computers & Geosciences*, 30(8):899–908, oct 2004. doi: 10.1016/j.cageo.2004.06.007. URL https://doi.org/10.1016%2Fj.cageo.2004.06.007.

P. Vallelonga, K. Christianson, R. B. Alley, S. Anandakrishnan, J. E. M. Christian, D. Dahl-Jensen, V. Gkinis, C. Holme, R. W. Jacobel, N. B. Karlsson, B. A. Keisling, S. Kipfstuhl, H. A. Kjær, M. E. L. Kristensen, A. Muto, L. E. Peters, T. Popp, K. L. Riverman, A. M. Svensson, C. Tibuleac, B. M. Vinther, Y. Weng, and M. Winstrup. Initial results from geophysical surveys and shallow coring of the Northeast Greenland Ice Stream (NEGIS). *The Cryosphere*, 8(4):1275–1287, jul 2014. doi: 10.5194/tc-8-1275-2014. URL https://doi.org/10.5194%2Ftc-8-1275-2014.

N. Wilkens, J. Behrens, T. Kleiner, D. Rippin, M. Rückamp, and A. Humbert. Thermal structure and basal sliding parametrisation at Pine Island Glacier – a 3-D full-Stokes model study. *The Cryosphere*, 9(2):675–690, apr 2015. doi: 10.5194/tc-9-675-2015. URL https://doi.org/10.5194%2Ftc-9-675-2015.

Anna Winter, Daniel Steinhage, Emily J. Arnold, Donald D. Blankenship, Marie G. P. Cavitte, Hugh F. J. Corr, John D. Paden, Stefano Urbini, Duncan A. Young, and Olaf Eisen. Comparison of measurements from different radio-echo sounding systems and synchronization with the ice core at Dome C Antarctica. *The Cryosphere*, 11(1):653–668, mar 2017. doi: 10.5194/tc-11-653-2017. URL https://doi.org/10.5194%2Ftc-11-653-2017.

A. P. Wright, D. A. Young, J. L. Roberts, D. M. Schroeder, J. L. Bamber, J. A. Dowdeswell, N. W. Young, A. M. Le Brocq, R. C. Warner, A. J. Payne, D. D. Blankenship, T. D. van Ommen, and M. J. Siegert. Evidence of a hydrological connection between the ice divide and ice sheet margin in the Aurora Subglacial Basin East Antarctica. *Journal of Geophysical Research: Earth Surface*, 117(F1):n/a–n/a, mar 2012. doi: 10.1029/2011jf002066. URL https://doi.org/10.1029%2F2011jf002066.

D. A. Young, D. M. Schroeder, D. D. Blankenship, Scott D. Kempf, and E. Quartini. The distribution of basal water between Antarctic subglacial lakes from radar sounding. *Philosophical Transactions of the Royal Society A: Mathematical Physical and Engineering Sciences*, 374(2059):20140297, jan 2016. doi: 10.1098/rsta.2014.0297. URL https://doi.org/10.1098%2Frsta.2014.0297.